TELOMERASE DEPLETION ACCELERATES AGEING OF THE ZEBRAFISH BRAIN

Raquel R. Martins[1,3], Savandara Besse[3], Pam S. Ellis[1], Rabia Sevil[4], Naomi Hartopp[3], Catherine Purse[1], Georgia Everett-Brown[1], Owain Evans[1], Nadiyah Mughal[1], Mina HF Wahib[1], Zerkif Yazigan[1], Samir Morsli[1], Ada Jimenez-Gonzales[3], Andrew Grierson[3], Heather Mortiboys[3], Chrissy Hammond[4], Michael Rera[2] and Catarina M. Henriques[1]

1. School of Medicine and Population Health, Bateson Centre for Disease Mechanisms and Healthy Lifespan Institute (HELSI), University of Sheffield, UK
2. Institut Jacques Monod (UMR7592), Paris, France.
3. Sheffield Institute for Translational Neuroscience (SITraN), University of Sheffield, UK
4. School of Physiology, Pharmacology and Neuroscience, University of Bristol, UK

Corresponding author: c.m.henriques@sheffield.ac.uk

GRAPHICAL ABSTRACT

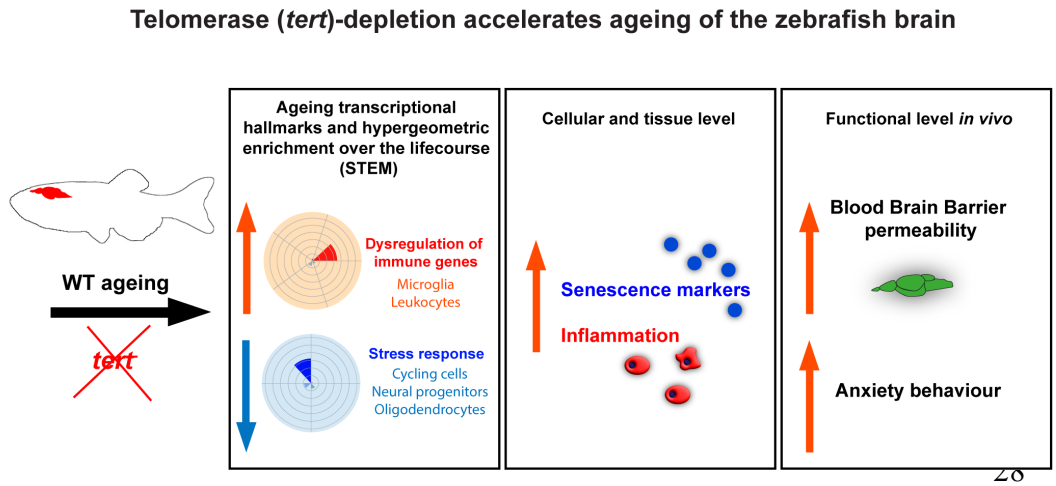

Graphical Abstract: Telomerase depletion accelerates markers of ageing in the zebrafish brain, ranging from dysregulated immune and stress ageing transcriptomic hallmarks to *in situ* accumulation of senescence-associated markers and inflammation, dysfunction of the blood-brain barrier and increased anxiety behaviour.

ABSTRACT

Decreased telomerase expression, telomere shortening, senescence-associated markers and inflammation have all been independently observed in the ageing brain and associated with disease. However, causality between limited telomerase expression and brain senescence and neuro-inflammation in the natural ageing setting is yet to be established. Here, we address these questions using the zebrafish as an ageing model which. Akin to humans, zebrafish display premature ageing and death in the absence of telomerase and where telomere shortening is a driver of cellular senescence.

Our work shows for the first time that telomerase deficiency (*tert*$^{-/-}$) accelerates key hallmarks of ageing identified in the Wild Type (WT) zebrafish brain at transcriptional, cellular, tissue and functional levels. We show that telomerase depletion accelerates ageing-associated transcriptomic changes associated with dysregulation of stress response and immune genes. These are accompanied by accelerated *in situ* accumulation of senescence-associated markers and inflammation in the aged brain. Importantly, *In vivo*, these changes correlate with increased blood-brain barrier permeability and increased anxiety-like behaviour. Of note, the acceleration of senescence-associated markers in the absence of tert occurs not only in the expected proliferative areas but also in non-proliferative ones, where it is unlikely due to telomere-dependent replicative exhaustion, suggesting that non-canonical roles of telomerase may be involved.

Together, our work suggests that telomerase has a protective role in the zebrafish brain against the accumulation of senescence and neuro-inflammation and is required for blood-brain barrier integrity.

KEY WORDS: Zebrafish, telomerase, TERT, ageing, brain, inflammation, Blood-brain barrier (BBB), senescence, behaviour, transcriptomics

ABBREVIATIONS:

AD, Alzheimer's disease

ALS, amyotrophic lateral sclerosis

67 ANOVA, analysis of variance

68 ATH, ageing transcriptional hallmarks

69 BBB, blood-brain barrier

70 BCA, bicinchoninic acid

71 bp, base pair

72 BSA, bovine serum albumin

73 Ce, cerebellum

74 Cent, centromere

75 CNS, central nervous system

76 DAPI, 4',6-diamidino-2-phenylindole

77 DAVID, database for annotation, visualization, and integrated discovery

78 DDR, DNA damage response

79 DEG, differential expression gene

80 Die, diencephalon

81 dH2O, distilled water

82 DNA, deoxyribonucleic acid

83 Dpf, day post fertilisation

84 dscDNA, double-stranded cDNA

85 EDTA, ethylenediaminetetraacetic acid

86 ENU, N-ethyl-N-nitrosourea

87 FAM, carboxyfluorescein

88 FISH, fluorescence *in situ* hybridisation

89 GEO, gene expression omnibus

90 GOBP, gene ontology biological pathway

91 h, hours

92 HBSS, Hanks buffered solution

93 IF, immunofluorescence

94 IP, intraperitoneal injection

95 IR, irradiation

96 KCN, potassium cyanide

97 KEEG, Kyoto encyclopaedia of genes and genomes

98 KH_2PO_4, potassium dihydrogen phosphate

99 KO, knock-out

100 LCP1, Lplastin

101 LMF, Wolfson light microscopy facility

102 LPS, lipopolysaccharide

103 MgCl2, magnesium chloride

104 Min, minutes

105 MO, medulla oblongata

106 NaCl, sodium chloride

107 NADH, nicotinamide adenine dinucleotide reduced disodium salt

108 NFkβ, nuclear factor kappa β

109 nm, nanometers

110 NO, novel object

111 NPCs, neural progenitor cells

112 NSCs, neural stem cells

113 O.C.T., mounting media

114 OT, optic tectum

115 PBS, phosphate buffered saline

116 PCA, principal component analysis

117 PCNA, proliferating cell nuclear antigen

118 PFA, paraformaldehyde

119 PNA, peptide nucleic acid

120 RIN, RNA integrity number

121 RNA, ribonucleic acid

122 RPM, revolutions per minute

123 RT, room temperature

124 SASP, senescence-associated secretory phenotype

125 sec, seconds

126 SITraN, Sheffield Institute for Translational Neuroscience

127 SSC, saline-sodium citrate

128 TE, Tris-EDTA

129 Tel, telencephalon

130 Telo, telomere

131 Tert, telomerase

132 TERT, telomerase reverse transcriptase

133 TNFα, tumour necrosis factor alpha

134 WT, wild-typeZIRC, Zebrafish international resource center

135 4-MU-chitotrioside , 4–methylumbelliferyl–β-D-N, N', N"-triacetylchitotriose

136 2,6-DCPIP, 2,6-dichlorobenzenone-indophenol sodium salt

137

138 **1 INTRODUCTION**

139 Brain ageing and related neurodegenerative diseases have dramatic consequences on
140 quality of life and medical care costs. Dementia alone, one of the most prevalent
141 manifestations of neurodegenerative disease affects 23 million people in the UK alone at a
142 cost of around £26 billion a year to the NHS [1-3]. Understanding the mechanisms underlying

143 brain ageing will target multiple age-associated brain diseases rather than one disease,
144 aiming to ameliorate quality of life in the elderly.
145
146 There are well-known key hallmarks of ageing which include telomere attrition, cellular
147 senescence, stem cell exhaustion and chronic inflammation amongst others[4,5]. Telomeres
148 are (TTAGGG)n DNA repeats that together with a complex of proteins (known as Shelterin)
149 create a “cap-like” structure at the end of linear chromosomes[6], preventing the ends of linear
150 chromosomes from being recognised as deleterious DNA double strand breaks[7]. However,
151 in humans, due to time- and cell-specific-limited telomerase expression, telomeres shorten
152 with each cell division, eventually leading to proliferative exhaustion and replicative
153 senescence[8,9]. Even though senescent cells do not proliferate, they are metabolically active,
154 releasing several inflammatory factors, tissue remodelling factors and growth factors, known
155 as Senescence Associated Secretory Phenotype (SASP)[10]. Consequently, accumulation of
156 senescent cells can contribute to impairment of tissue homeostasis, a low level of chronic
157 inflammation and have been linked to several age-associated diseases[11,12]. Importantly,
158 cellular senescence accumulates with ageing in humans, and this can be thought of as a
159 general stress response[13-15].
160
161 Restricted telomerase expression and consequent telomere dysfunction function are key
162 hallmarks of natural ageing in humans, underpinning multiple age-related diseases[16]. As
163 tissues with high cellular turnover present accelerated telomere erosion[8,17], it is reasonable
164 to speculate that telomerase functions are likely to primarily affect highly proliferative
165 tissues. Accordingly, premature accumulation of critically short telomeres has been
166 identified in highly proliferative tissues such as the gut, in tert-deficient animal models,
167 including first generation zebrafish *tert*$^{-/-}$ mutants (and late generation TERT KO mice)[17-20].
168 Nevertheless, because senescence has been shown to "spread", in a phenomenon described
169 as paracrine senescence, telomere-dependent genome instability and replicative senescence
170 may lead to non-cell autonomous increase in senescence-associated markers and
171 inflammation[21]. This means that the role of telomerase and telomeres is not restricted to
172 highly proliferative tissues. To complicate things further, growing evidence suggests that the
173 Tert component of telomerase also has non-canonical activities, independent of its action at
174 telomeres[22-25]. In the nucleus, these non-canonical functions include transcriptional

175 regulation of genes involved in inflammation, including nuclear factor kappa β (NFkβ) and
176 tumour necrosis factor alpha (TNFα)[26-28] as well as genes involved in cell proliferation[29,30] and
177 cell survival[31,32]. Telomerase can also translocate to the mitochondria, where it has been
178 shown to play a protective role against DNA damage and oxidative stress[33,34]. In the brain,
179 considered a predominantly post-mitotic tissue, telomerase has been shown to have a
180 protective role against excitotoxicity[35], oxidative stress[36] and neuronal death[37] all involved
181 in neurodegenerative diseases. Studies in late-generation telomerase-deficient mice have
182 suggested that limited telomerase expression is associated with premature accumulation of
183 senescence-associated markers in different cell populations in the CNS, including Purkinje
184 neurons, cortical neurons and microglia[38-41]. However, it is still unclear whether this is due
185 to telomere length maintenance or non-canonical functions of telomerase[29,30].
186
187 There are many different stimuli that can cause cellular senescence, including epigenetic
188 alterations, oxidative stress, mitochondrial dysfunction, inactivation of tumour suppressor
189 genes, mechanical or shear stress, pathogens, and activation of oncogenes[42,43]. What causal
190 role telomerase and telomere dysfunction plays in CNS senescence in humans is, however,
191 not clear, even if implicated[44]. Nevertheless, telomere shortening has been associated with
192 neurodegenerative diseases, including Parkinson's and AD[45], including via glia activation and
193 pathogenesis[46]. Of note, a recent study analysing human brain biobank data from over
194 30,000 patients identified a positive correlation between shorter leukocyte telomere length
195 (used as a proxy for the patient's general telomere length) and neurodegenerative
196 phenotypes[47]. Additionally, cellular senescence-associated markers have been reported in
197 human neuroinflammation and neurodegenerative diseases. Increased levels of DNA
198 damage checkpoints such as p53, p21 and p16, as well as SASP factors have been observed
199 in the spinal cord and brain of patients with amyotrophic lateral sclerosis (ALS)[38] and
200 Alzheimer’s disease (AD)[48], respectively. Higher mRNA levels of p16INK4a in the substantia
201 nigra pars compacta (SNpc) were also observed in post-mortem tissue of patients with
202 Parkinson’s disease (PD) compared to healthy controls[49]. Moreover, senescence,
203 neuroinflammation and oligomeric tau have been associated with AD pathology, recently
204 reviewed here[50]. Hence, growing evidence suggest that, despite being a low proliferative
205 tissue, the CNS accumulates senescence or at least senescence-associated markers, and that
206 this may be associated with brain diseases of ageing. However, causality between limited

207 telomerase expression and increased senescence and neuro-inflammation in the natural
208 ageing setting is yet to be established. Nevertheless, reducing putative senescent cells leads
209 to improvement of cognitive decline in aged mice, suggesting an active role for senescence
210 in this phenotype[51]. It remains to be determined which cell populations undergo senescence
211 in natural ageing, in the CNS, and what type of senescence this is, i.e., replicative (telomere-
212 dependent) or stress-induced senescence. Understanding whether and how telomerase
213 restriction may contribute to ageing-associated brain degenerative phenotypes would help
214 understand the fundamental mechanisms of brain functional decline and potentially
215 contribute to the uncovering of new therapeutic targets to delay or prevent disease.
216
217 The role of telomerase restriction and its consequences in natural ageing may benefit from
218 additional and complementary models, beyond the mouse, where most lab-strains have
219 significant longer telomeres than humans and show little evidence of replicative
220 senescence[52,53]. The zebrafish may offer such a model since, like in humans, telomerase
221 depletion leads to significant decrease in health and lifespan[18-20,54]. As it was shown that the
222 zebrafish brain presents low levels of Tert in the adult brain and that these decrease further
223 with ageing[55,56], we hypothesised that limited expression of Tert in the aged zebrafish brain
224 contributes to brain degeneration with ageing. To our knowledge, this manuscript represents
225 the first broad characterisation of zebrafish brain ageing in the presence and absence of
226 telomerase (Tert).
227
228 To test our hypothesis, we performed RNA sequencing in whole brains of zebrafish
229 throughout their lifecourse in both the presence and absence of telomerase (tert).
230 Specifically, we compared WT and *tert*$^{-/-}$ siblings derived from tert$^{+/-}$ in-crosses at the age
231 ranges of 2-6, 9-16 and 18-24 for WT and *tert*$^{-/-}$ and up to 30-36 months in WT only, since the
232 *tert*$^{-/-}$ do not live past 18-24 months. *tert*$^{-/-}$ zebrafish, extensively characterised elsewhere
233 [18,19,57], display no telomerase activity and have significantly shorter telomeres from birth,
234 consequently ageing and dying prematurely. Ageing is usually described as a time-dependent
235 change in tissue homeostasis, that increases the probability of disease and death[58]. However,
236 whether the genes and pathways driving or accompanying these time-dependent changes
237 are also consistently changing in a time-specific manner, remains unresolved [59]. We
238 therefore decided to combine a time-series analysis (STEM), which allowed the identification

239 of genes and pathways that are consistently up or down-regulated over-time, with the more
240 traditional differential gene expression (DEGs) analysis between young and old animals. This
241 combined strategy allowed the identification of genes that change in a monotonic, time-
242 dependent manner (STEM), versus genes that change at specific stages of life (DEGs). Both
243 transcriptomic analyses strategies, combined with enrichment strategies highlighted
244 increased immune response and decreased proliferation as the main signatures of ageing in
245 both WT and *tert*$^{-/-}$ zebrafish brains. We then asked which specific WT ageing-associated
246 gene changes (STEM and standard DEG comparisons between time points) were accelerated,
247 i.e., occurred at an earlier age, in the absence of telomerase (tert). The more refined STEM-
248 based analyses identified 6 specific gene changes accelerated from the age of 9-16 months
249 in *tert*$^{-/-}$ and 11 from the age of 18-24, contrasting to 30-36 months in WT. Broader DEG
250 comparisons-based analyses were used to identify DEGs of "old age" (WT young *VS* old) and
251 then compared with *tert*$^{-/-}$ at the different ages to determine how telomerase depletion may
252 accelerate transcriptomic changes of "old age". This approach identified 4 DEGs accelerated
253 from the early age of 2-6 months in *tert*$^{-/-}$; 639 from the age of 9-16 and 109 from the age of
254 18-24. These transcriptomic changes were accompanied by an *in situ* acceleration of
255 senescence-associated markers and inflammation. *In vivo*, telomerase depletion accelerated
256 ageing-associated increased in blood-brain barrier permeability and increased anxiety-like
257 behaviour. Together, our work suggests that telomerase has a protective role in the zebrafish
258 brain against the accumulation of senescence and neuro-inflammation and is required for
259 BBB integrity.
260

261 **2 RESULTS**

262 **2.1 Telomerase (tert) depletion accelerates transcriptomic changes of ageing in the**
263 **zebrafish brain**

264 Tissue-specific transcriptomic analysis over the life course can offer important insights into
265 the downstream molecular mechanisms underpinning age-associated pathologies.
266 Significant research is being dedicated to these approaches in different animal models,
267 including in mice[60-62]. To identify telomerase-dependent and -independent transcriptional
268 signatures of ageing in the zebrafish brain, we performed RNA-Sequencing of whole brain
269 tissue, throughout the lifespan of WT and telomerase-deficient (*tert*$^{-/-}$) fish (**Fig. 1** and
270 supplementary source data files). While *tert*$^{-/-}$ fish have a lifespan of c. 18-24 months, WT fish

271 typically die between c. 36-42 months of age [20]. The data shown here include 4 age-groups
272 of WT (2-6, 9-16, 18-24 and 30-36 months), corresponding to young, adult, median lifespan
273 and old, respectively. As the *tert*$^{-/-}$ fish have a shorter lifespan compared with their WT
274 siblings, the data include 3 age-groups of telomerase-deficient fish (2-6, 9-16, and 18-24
275 months), which correspond to young, medium lifespan and old (see Materials & Methods for
276 further explanation of genotypes and ages chosen) (**Fig 1A**). The reads were aligned to the
277 latest zebrafish genome build GRCz11[63] and resulted in uniquely mapped read percentages
278 ranging from 92.1% to 94.4%, which is considered good quality[63]. All samples had at least 10
279 million uniquely mapped reads. To analyse the overall impact of the genotype and age on
280 transcriptomic regulation, we performed a Principal Component Analysis (PCA) and observed
281 that the samples cluster mainly *per* age (**Supp Fig 1A**).
282
283 We performed a time-series analysis (STEM) (**Fig 1** and supplementary source (SS) data),
284 which allowed the identification of genes and pathways that are consistently up or down-
285 regulated over-time. In parallel, we performed a broader, more traditional differential gene
286 expression (DEGs) analysis at the different time-points, in WT and *tert*$^{-/-}$ (**Supp Fig 1** and SS
287 data). For the time-series analysis, we grouped the gene expression data into temporal
288 expression profiles using Short Time-series Expression Miner (STEM) software[64]. To
289 determine whether the temporal profiles were associated with specific biological processes
290 and pathways, pathway over-representation analysis (ORA) were performed for the genes
291 assigned to the significant STEM profiles. In the WT brain, we identified 6 temporal profiles,
292 3 of them including overall up-regulated genes (profiles 40, 18 and 29), and 3 including
293 overall down-regulated genes (profiles 1, 26 and 15). In the *tert*$^{-/-}$ brain, time-series analysis
294 revealed 5 different profiles. Profiles 8 and 15 containing overall up-regulated genes and
295 profiles 0, 7 and 3 containing overall down-regulated genes (**Fig. 1B** and SS data). We then
296 performed two types of enrichment analyses strategies: Gene Ontology Biological Pathway
297 (GOBP) and hypergeometric. GOBP analysis of STEM profiles highlighted up-regulation of
298 immune response and downregulation of cell-cycle and related pathways with ageing in both
299 WT and *tert*$^{-/-}$ zebrafish brains (**Fig 1B1**). The hypergeometric enrichment analysis allowed
300 us to further investigate the cellular context of age-associated transcriptional changes. To do
301 this, we mapped the gene sets from significant STEM profiles in WT and *tert*$^{-/-}$ mutant brains
302 onto a published zebrafish brain single-cell dataset[65]. This dataset was chosen because it

303 provides high-quality profiles (>16,000 cells at ~8,000 UMIs per cell), detailed annotations of
304 unsorted cells capturing the full cell repertoire, and accessible raw and processed data. In
305 WT brains, the major downregulated trajectory (STEM profile 1) was most strongly enriched
306 for genes expressed in cycling cells, with lesser enrichment in neural progenitor cells (NPCs),
307 and oligodendrocytes, indicating a decline in proliferative and myelinating populations with
308 age. Similarly, in *tert*$^{-/-}$ mutants, multiple downregulated profiles (0, 3, and 7) showed
309 enrichment for cycling cells, NPCs, oligodendrocytes, and additionally in differentiating
310 oligodendrocyte progenitor cells (OPCs). In contrast, upward trajectories in both WTs
311 (profiles 18, 29, and 40) and *tert*$^{-/-}$ mutants (profiles 8 and 15), were enriched for leukocytes
312 and microglia, consistent with increased immune activity during ageing (**Fig 1B2**). These
313 enrichment analyses were further supported when we contextualise pathway enrichments
314 within the hallmarks of ageing, using a previously described strategy[66] (see additional details
315 in Materials and Methods). Here, we mapped known GOBP terms to experimentally
316 identified ageing transcriptomic hallmarks (ATH)[67]. ATH mapping identified dysregulation of
317 immune genes (ATH1) in up-regulated STEM profiles and stress response (ATH2) in down-
318 regulated STEM profiles in both WT and *tert*$^{-/-}$ zebrafish (**Fig 1C** and SS data). The broader
319 analysis of "DEGs of old age" (WT young VS old) showed a GOBP enrichment for cell cycle,
320 division, chromatin-organisation and chromosome segregation and downregulation of DNA
321 transcription as the top 5 enriched pathways. Notably, when mapped to ATH, this broader
322 analysis identified dysregulation of gene expression, stress response and dysregulation of
323 immune genes as the top 3 hallmarks of old age[67] (**Supp Fig 1** and SS data), supporting the
324 STEM analysis. We further validated selected DEGs of old age by RT-QPCR (*ctss2.1* and *parp3*)
325 and/or *in situ* hybridisation (*cdkn2a/b "p16-like* and *cdkn1a "p21-like"*) (**Fig 2B3** and **Supp Fig**
326 **4**).
327
328 Finally, we asked which specific WT ageing-associated gene changes from the STEM and
329 standard DEG comparisons between time points) were accelerated in the absence of
330 telomerase (*tert*$^{-/-}$), i.e., occurred at an earlier age than WT. The more refined STEM-based
331 analyses identified 6 specific gene changes accelerated from the age of 9-16 months in *tert*$^{-}$
332 $^{/-}$ and a further 11 from the age of 18-24 months, contrasting to old WT (30-36 months).
333 These included namely down-regulation of SI:DKEY-225F5.4 (an ortholog to ZWINT human
334 gene) and ZGC:101100 (aka dmbx2 in zebrafish and

335 diencephalon/mesencephalon homeobox 2) and upregulation of *klf9* (Kruppel like factor 9,
336 *lyn* (LYN proto-oncogene, Src family tyrosine kinase), mhc1uka (major histocompatibility
337 complex class I UKA) and mxc (myxovirus (influenza virus) resistance C) accelerated from the
338 ages of 9-16 months in *tert*$^{-/-}$. We identified a further 11 from the age of 18-24, contrasting
339 to 30-36 months in WT (**Fig 1C** and SS data). We performed a similar analysis using the
340 broader "DEGs of old age" (**Supp Fig 1C** and SS data). To do this, we compared DEGs identified
341 in *tert*$^{-/-}$ zebrafish brains over time (i.e. 2-6 *VS* 9-16 months and 2-6 *VS* 18-14 months) with
342 the WT "DEGs of old age". We then selected only the ones that changed in *tert*$^{-/-}$ in the same
343 direction as WT, i.e., either up or downregulated and further compared these with the
344 corresponding age in sibling WT DEGs, to check whether they were accelerated in *tert*$^{-/-}$, i.e.,
345 changed at younger ages than the equivalent sibling WT. Using this strategy, we identified
346 1049 DEGs of old age accelerated in the absence of telomerase (*tert*$^{-/-}$), which comprised
347 c.36% of the total (2887) "DEGs of old age" (**Supp Fig 2** and SS data). Within these, 4 "DEGs
348 of old age" were accelerated from the early age of 2-6 months in *tert*$^{-/-}$; 639 from the age of
349 9-16 and 109 from the age of 18-24, contrasting with the age of 30-36 in WT. Notably, when
350 mapped to the ageing transcriptomic hallmarks of ageing, the "DEGs of old age" accelerated
351 in the absence of telomerase identified dysregulation of gene expression, stress response
352 and dysregulation of immune genes as the top 3 significantly enriched transcriptional
353 hallmarks[67], similarly to the overall DEGs of WT old, and to similar extents (**Supp Fig 3** and SS
354 data).

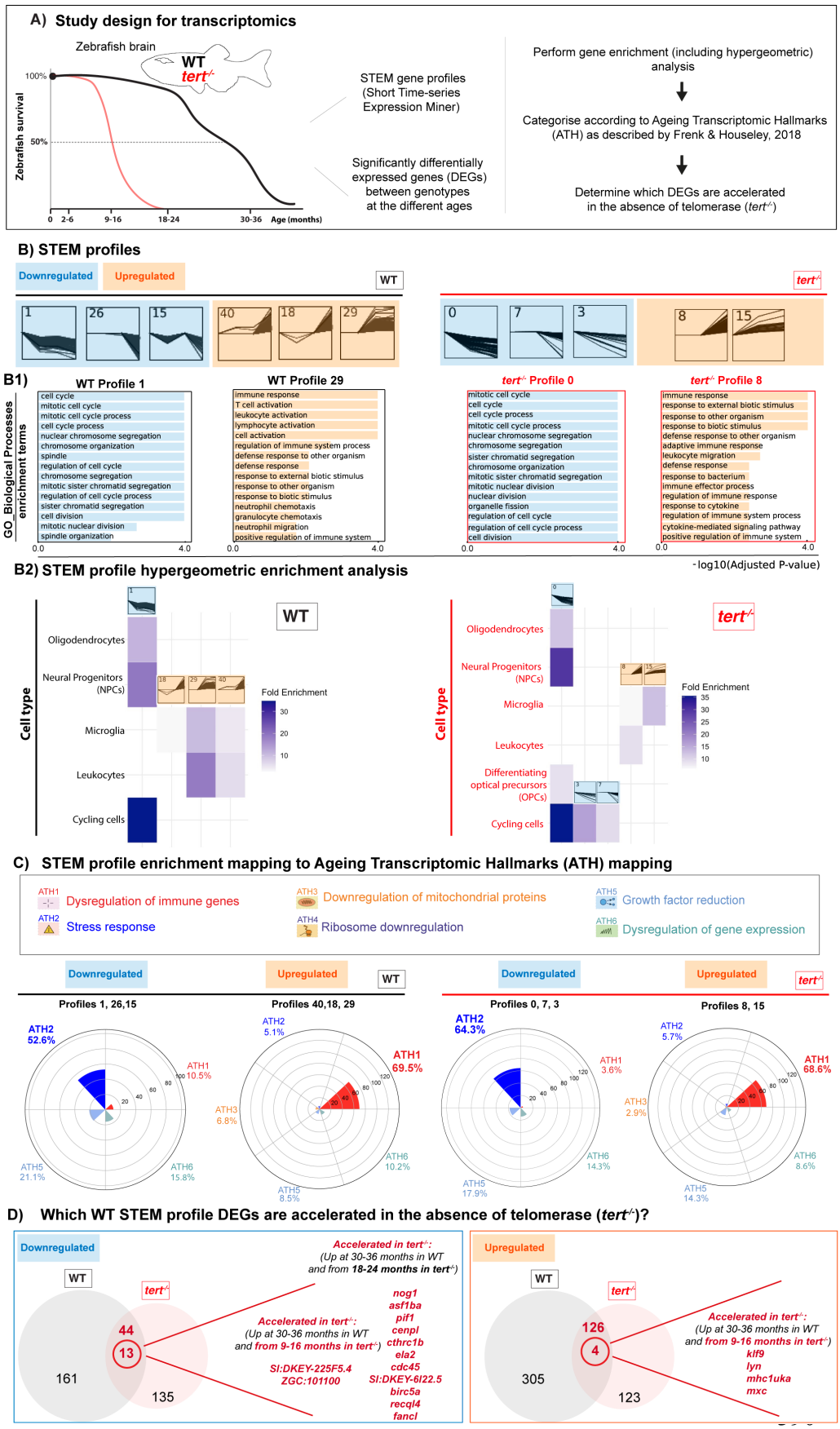

Figure 1. Transcriptomic signatures of ageing in the presence and absence of telomerase in the zebrafish brain. (A) Schematic figure of the study design for transcriptomics: RNA from whole brain tissue from young

393 (ca. 2-6 months), young adult (ca. 9-16 months), middle aged (ca. 18-24 months) and old (,30-36 months) WT
394 fish, and young (ca. 2-6 months), middle aged (ca. 9-16 months) and old (ca. 18-24 months) *tert*$^{-/-}$ fish was used
395 for RNA sequencing. N=3 per group. Transcriptomic alterations of ageing were analysed using two
396 complementary approaches: STEM profiles and traditional DEG analysis between genotypes at different ages.
397 Enrichment analysis and hypergeometric analysis were performed to identify the predominant pathways
398 altered with ageing in the presence and absence of telomerase, and the DEGs were mapped to the ageing
399 transcriptomic hallmarks (ATH). (B) Plots of the profiles identified by the STEM analysis (profiles containing
400 down-regulated genes in blue and profiles containing up-regulated genes in orange) in both WT and *tert*$^{-/-}$
401 zebrafish brains, and (B1) top enrichment pathways (GOBP) identified in representative profiles. (B2) STEM
402 profile hypergeometric enrichment analysis in WT and *tert*$^{-/-}$ brains identified which cell populations are mainly
403 affected with ageing in the presence and absence of telomerase. (C) The genes identified by STEM analysis
404 were then mapped to ATH. Plots show the proportion of genes mapped to each ATH, in both WT and *tert*$^{-/-}$ fish.
405 (D) Venn diagrams highlight the genes identified in the STEM profiles of WT fish that are accelerated in the
406 absence of telomerase (i.e. in *tert*$^{-/-}$ fish).
407
408
409 **2.2 Telomerase (tert) depletion accelerates ageing-associated stress response in the**
410 **zebrafish brain**
411 Given our transcriptomic analysis results in 2.1, we proceeded to testing whether these
412 changes were reflected at cell and tissue level starting with markers associated with the
413 "stress response" transcriptomic hallmark of ageing: cell cycle (also highlighted in both the
414 GOBP and the hypergeometric analysis); senescence-associated markers; DNA damage
415 response and relative telomere length, in brain sections of WT and *tert*$^{-/-}$ zebrafish over their
416 lifecourse.
417
418 There is not a single marker that can be used on its own to irrefutably identify a senescent
419 cell and markers often described to be associated with senescence in proliferative tissues,
420 such as P16 and P21, are highly expressed in terminally differentiated neurons[68,69]. This may
421 confound identification of putative senescent cells. Nevertheless, markers such as P16 have
422 previously identified as a good marker for predicting disease progression in Parkinson's
423 Disease (PD) patients[70], and with ageing[71]. Acknowledging these limitations, we performed
424 a broad characterisation of putative cellular senescence as a stress response using the
425 following **5 main readouts**[42] (Hernandez-Segura et al., 2018) (**Fig 2B**): **1)** accumulation of
426 Senescence-Associated β Galactosidase (SA-β-Gal) a known biomarker of cellular

427 senescence, at least in most of the cell types tested[13], and often present in different types of
428 senescence (**Fig 2B1-3**); **2)** levels of expression of cell cycle kinase inhibitors *p21* and *p16*
429 genes (**Fig 2B2, B4 and Supp Fig 4B**); **3)** proliferation, by Proliferating Cell Nuclear Antigen
430 (PCNA) expression and EdU pulse chase labelling (**Fig 2B2, B5 and C**); **4)** DNA Damage
431 Response (DDR) by identifying cells with strong signal reflecting multiple γH2AX foci (**Supp**
432 **Fig 5**) and **5)** relative telomere length (**Fig 2 D and Supp Fig 5B**).
433
434 Our initial whole brain SA-β-Gal staining in WT zebrafish brains detected more intense blue
435 staining in WT old (30-36 months), when compared to young (2-6 months), which motivated
436 us to explore further (**Fig 2A**). To do this, we dissected and sectioned a separate set of brains
437 to determine which regions had increased SA-β-Gal staining, comparing WT and *tert*$^{-/-}$
438 siblings at different ages. Our results showed a significant increase in SA-β-Gal with ageing
439 in specific regions of the WT zebrafish brain, such as in the midline of the telencephalon,
440 diencephalon, cerebellum and medulla oblongata (**Fig 2B1**). Accumulation of SA-β-Gal in the
441 diencephalon, cerebellum and medulla oblongata was significantly accelerated in the
442 absence of telomerase (*tert*$^{-/-}$), where, at 2-6 months, the *tert*$^{-/-}$ brain is already displaying
443 the pattern and levels of SA-β-Gal observed in old WT brains of 30-36 months of age
444 (diencephalon quantification shown as a representative example in **Fig 2B2**).
445
446 We then collected 2 further sets of zebrafish WT and *tert*$^{-/-}$ sibling brains to assess a)
447 *cdkn2a/b* "*p16-like" (RNA in situ),* PCNA (IF) *and* SA-βgal (chromogenic) (**Fig 2**) and b) *cdkn1a*
448 "*p21-like"* and *cdkn2a/b* "*p16-like"* genes (RNA *in situ)* (alongside a repeat of chromogenic
449 SA-βgal as control) (**Supp Fig 4**) in sequential sections of the respective animals. Our data
450 show an increase in *cdkn2a/b* "*p16-like"* expression levels with ageing in WT and *tert*$^{-/-}$, this
451 is not accelerated by the absence of telomerase, either at 2-6 or 9-16 months (**Fig 2B and**
452 **B4**). Notably, the increase in *cdkn2a/b* "*p16-like"* expression was not accompanied by *cdkn1a*
453 "*p21-like"* expression (**Supp Fig 4B**). We detected very little proliferation in the zebrafish
454 brain—generally under 5% of PCNA+ cells per FOV in any region we looked (**Supp Fig 5A**).
455 Even after 3 days pulse with EdU, the % of EdU^{+} cells in the diencephalon/Optic tectum,
456 where known proliferative niches reside), was under 1%/ FOV (**Fig 2C**). Nevertheless, both
457 PCNA and EdU data show a significant decrease in proliferating cells with ageing in both WT

458 and *tert*$^{-/-}$ in the diencephalon/optic tectum (PCNA and EdU), but this is not significantly
459 accelerated in the absence of telomerase at the ages tested.
460
461 Another common marker of senescent cells is the accumulation of DNA damage response
462 (DDR) markers, such as γH2AX foci. Our data show that very few cells accumulate γH2AX foci
463 in the aged brain, in all regions tested (never more than 2% of cells (**Supp Fig 5A**).
464 Nevertheless, we detected a significant increase in γH2ax^{+} cells with ageing in both WT and
465 *tert*$^{-/-}$ in the cerebellum (**Supp Fig 5A2**) and when we combine diencephalon with Optic
466 Tectum regions (**Fig 2B6**). Notably, accumulation of DDR with ageing is accelerated in the
467 absence of telomerase in these brain regions from the age of 9-16 months in *tert*$^{-/-}$ zebrafish.
468 Of note, the senescence-associated markers tested (increase in SA-β-Gal, *cdkn2a/b "p16-*
469 *like"* and γH2AX^{+} cells) occur in both proliferative and non-proliferative areas of the brain
470 (**Fig 2B3)** (see example of ventral diencephalon and dorsal diencephalon, respectively, in a
471 young WT brain (**Fig 2 B3.1**).
472
473 To test whether increase in senescence-associated markers correlated with shorter
474 telomeres (i.e. putative replicative senescence), we measured relative telomere length in
475 brain sections of WT fish over time, alongside their *tert*$^{-/-}$ counterparts as previously
476 described by us, using a telomeric Peptide Nucleic Acid (PNA) probe alongside a centromeric
477 PNA probe in Fluorescence *in situ* Hybridisation (FISH)[72] (**Fig 2D** and **Supp Fig 5B**). We show
478 that relative telomere length decreases with ageing in WT brains and this is accelerated in
479 the absence of telomerase, where telomeres are significantly shorter in *tert*$^{-/-}$ from the young
480 age of 2-6 months, as has been shown for multiple tissues[20]. However, as expected, relative
481 telomere length in the brain is significantly longer than in the highly proliferative gut
482 epithelia of the same individuals, both in WT and *tert*$^{-/-}$ at the ages tested.

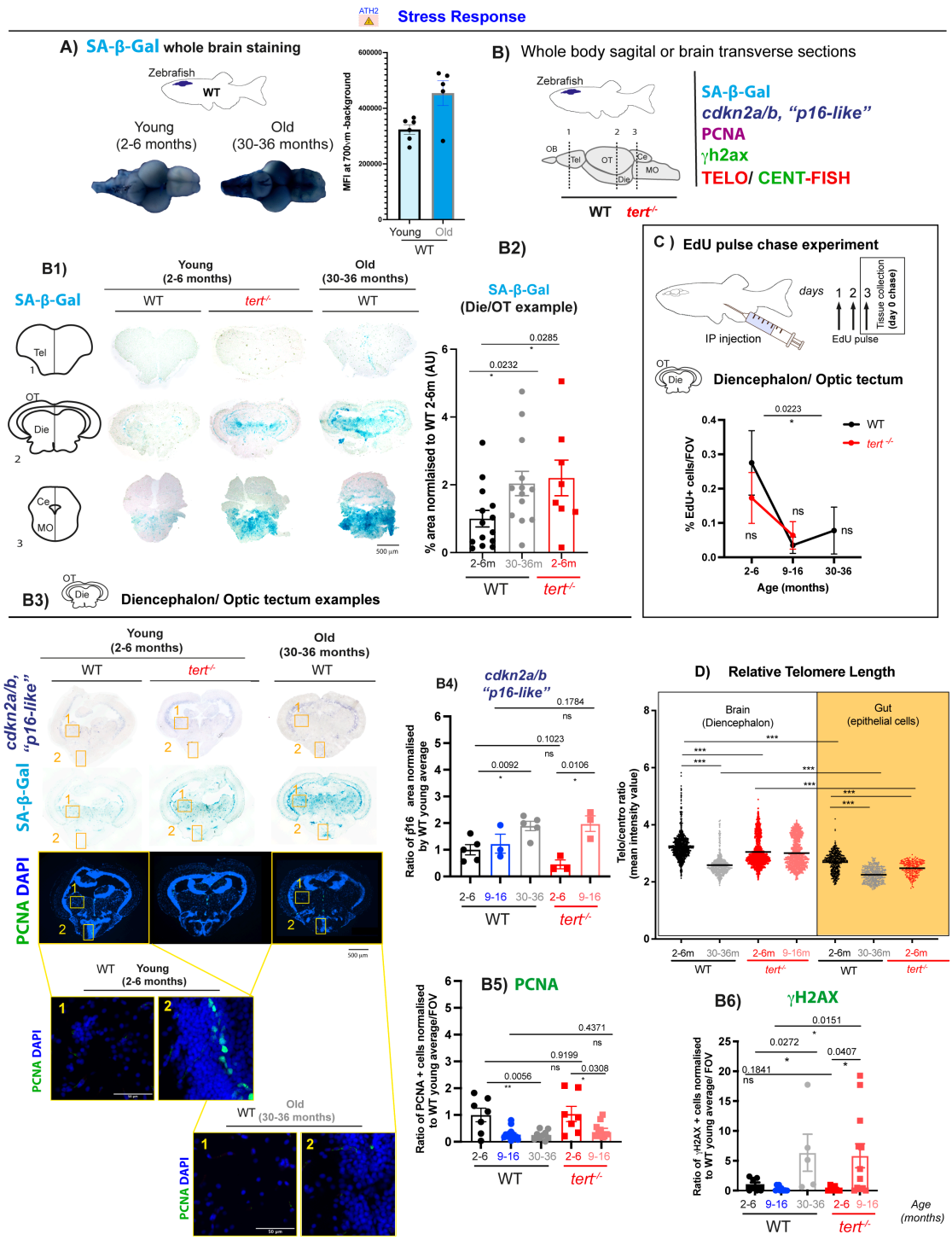

Figure 2. Telomerase (tert) depletion accelerates ageing-associated stress response in the zebrafish brain. Brain tissue collected from ca. 2-6 months, ca. 9-16 months and >30 months) WT fish, and ca. 2-6 months and ca. 9-16 months *tert*$^{-/-}$ fish were used to assess stress response by SA-β-Gal staining, *cdkn2a/b* ("*p16-like*") RNA expression, proliferation (PCNA and EDU staining), telomere length and DNA damage. (A) Whole brain SA-β-Gal staining in young and old WT fish and respective quantification show an increased expression of SA-β-Gal in old WT brains compared to young ones. N=5-6 per group. (B) Schematic figure showing the regions of the

490 brain assessed for senescence-associated markers. (B1) Representative images of SA-β-Gal staining in coronal
491 cryosections of WT and *tert*$^{-/-}$ zebrafish show that there is an increased expression of SA-β-Gal in old WT
492 zebrafish (>30 months) and that a similar pattern is observed in *tert*$^{-/-}$ at the young age of 2-6 months,
493 particularly in the diencephalon and optic tectum for which (B2) quantifications are shown. N=8-14 per group.
494 (B3) Representative images from *in-situ* hybridisation in coronal cryosections, show an increased expression of
495 *cdkn2a/b* ("*p16-like*") in WT zebrafish >30 months optic tectum and diencephalon, in areas where SA-β-Gal
496 expression is observed. This increase in *p16* expression is already significant at 9-16 months of age in *tert*$^{-/-}$.
497 Quantifications shown in B4. N=3-5 per group. (B3) Representative images of PCNA and γH2AX staining in
498 adjacent sections from zebrafish brain, in coronal cryosections. (B5) Proliferation assessed by PCNA staining
499 show a decrease in proliferation with ageing in both WT and *tert*$^{-/-}$ fish, and this is not accelerated in the absence
500 of telomerase. N=3-7 per group. (B6) DNA damage response assessed by γH2AX staining show increased DNA
501 damage in WT fish >30 months, this increase is anticipated in the *tert*$^{-/-}$ fish at 9-16 months but not at 2-6
502 months of age. N=3-7 per group. (C) Similar to what was observed by PCNA staining, proliferation assessment
503 by EDU staining after a 3-day pulse experiment show a decrease in proliferation with ageing in both WT and
504 *tert*$^{-/-}$ brains, but this is not anticipated in the absence of telomerase. N=3-7 per group. (D) Relative telomere
505 length, assessed by telo/cent-FISH, in longitudinal paraffin sections of zebrafish brain (white) and gut (yellow),
506 show that telomere length decreases with ageing in WT fish (>30 months) and that this is anticipated in young
507 *tert*$^{-/-}$ fish (ca. 2-6 months). N=4-5 per group. (A, B2, B4, B5, B6) Each dot represents one animal. (D) Each dot
508 represents one cell. Error bars: SEM. * $p<0.05$; ** $p<0.01$; *** $p<0.001$. Abbreviations: OB, olfactive bulb; Tel,
509 telencephalon; Die, diencephalon; OT, optic tectum; Ce, cerebellum; MO, medulla oblongata.
510
511 Different types of senescence stimuli have been identified to express different SASP factors.
512 We took advantage of available public databases of genes changes associated with SASP
513 factors in humans and mice (SASP atlas and Senmayo databases)[73,74] and compared them with
514 our transcriptomic STEM and broad "DEGs of old age". We were particularly interested in
515 determining whether any of these putative SASP-associated genes were accelerated in the
516 absence of telomerase, at the ages where we see acceleration of other senescence-associated
517 markers. The STEM-based SASP analysis identified 2 genes in common between WT and *tert*$^{-}$
518 $^{/-}$ profiles (*tyms* and *psm2*) (**Supp Fig 6A**), but none of these were accelerated in the absence
519 of tert (Fig 1 D).
520
521 However, when we performed the broader "DEGs of old age" accelerated in the absence of
522 telomerase, we identified a further 52 genes, including *psm2 (*accelerated in the absence of
523 telomerase from the age of 9-16 months*)*, which was also detected in the STEM profiles (**Supp**
524 **Fig 6B**). Of note, *idh1, lancl1, masp1, ncl and tuba1a* are accelerated in the absence of

525 telomerase from the age of 18-24 months, and the remaining ones from 18-24 months in *tert*$^{-}$
526 $^{/-}$ (SS data).
527
528 **2.3 Telomerase (tert) depletion accelerates ageing-associated inflammation in the**
529 **zebrafish brain**
530 We then proceeded to testing whether the changes associated with the "dysregulation of
531 immune response" ageing transcriptomic hallmark—also highlighted in both the GOBP and
532 hypergeometric analysis—were reflected at cell and tissue level starting. We started by
533 quantifying the percentage of immune cells in in brain sections of WT and *tert*$^{-/-}$ zebrafish
534 over their lifecourse.
535
536 Because there is no agreed specific microglia marker in zebrafish, we combined the
537 tg(*mpeg*1.1-mCherry-caax) transgenic zebrafish line[75], which has been shown to identify
538 macrophages and microglia in the brain[76] , with a well-described pan-immune cell marker (L-
539 plastin or LCP-1)[77-80] and use immunofluorescence (IF) to quantify immune cell populations
540 in the brain[81] as a readout for inflammation. Using these two markers allowed us to identify
541 macrophages/microglia as L-plastin^{+}*mpeg*$^{+}$ cells, and distinguish them from any other
542 immune cells, which would be L-plastin^{+}*mpeg*$^{-}$ (**Fig 3A).** Our data show that there is an
543 increased number of plastin^{+}*mpeg*$^{+}$ cells (**Fig 3A1**) but not of L-plastin^{+}*mpeg*$^{-}$ cells (**Fig 3A2**)
544 with ageing, in most of the zebrafish brain (WT 2-6 months *VS* WT 30-36 months) (**Supp Fig**
545 **7A**), suggesting a macrophage/microglia specific increase. The macrophage/microglia
546 increase in the brain with ageing (WT 2-6 months *VS* WT 30-36 months) is suggestive of
547 neuroinflammation and was accelerated in the absence of telomerase from the early age of
548 2-6 months (WT 2-6 months *VS tert*$^{-/-}$ 2-6 months), at which ages we do not see any
549 significant increase in immune cell proliferation (**Supp Fig 7B**).
550
551 To understand whether macrophage/microglia increase with ageing was associated with
552 immune activation, we used a chitotriosidase activity assay. Chitotriosidase is an enzyme
553 expressed by activated macrophages and other phagocytic cells and can therefore be used
554 as a biomarker of microglia/macrophage activation, including in zebrafish (Keatinge et al.,
555 2015). Our data show that there are increased levels of chitotriosidase in the naturally aged
556 brain (WT 2-6 *VS* 9-16 *VS* 30-36 months), suggesting age-associated neuronal immune

557 activation, which we show is accelerated in the absence of telomerase (*tert*$^{-/-}$) from the age
558 of 9-16 months (**Fig. 3B**).
559
560 Accumulation of cellular senescence is thought to contribute to chronic inflammation in
561 ageing, often termed "inflammageing"[82-84]. On one hand, in some contexts, immune cells
562 have been shown to be recruited to sites of cellular senescence[85,86]. On the other hand,
563 senescent cells have been shown to release pro-inflammatory factors (part of SASP), which
564 can contribute to paracrine senescence[87] as well as to tissue inflammation[83]. We therefore
565 set out to determine how the increased levels of senescence-associated markers we
566 detected in the zebrafish brain correlated with immune cell numbers. To do this, we
567 performed IF staining with the pan-immune cell marker L-plastin on SA-β-Gal-stained brain
568 tissue sections. Even though we cannot exclude that some of these immune cells may also
569 be SA-β-Gal^{+} themselves, most of the immune cells appear to surround, rather than overlap
570 with SA-β-Gal^{+} areas (**Fig 3C)** and there is a statistically significant positive correlation
571 between % of SA-β-Gal^{+} areas and % of immune cells with ageing in the WT zebrafish brain
572 (R^2=0.99), p(two-tailed) =0.0313.
573
574
575
576

A) % of immune cells in the brain

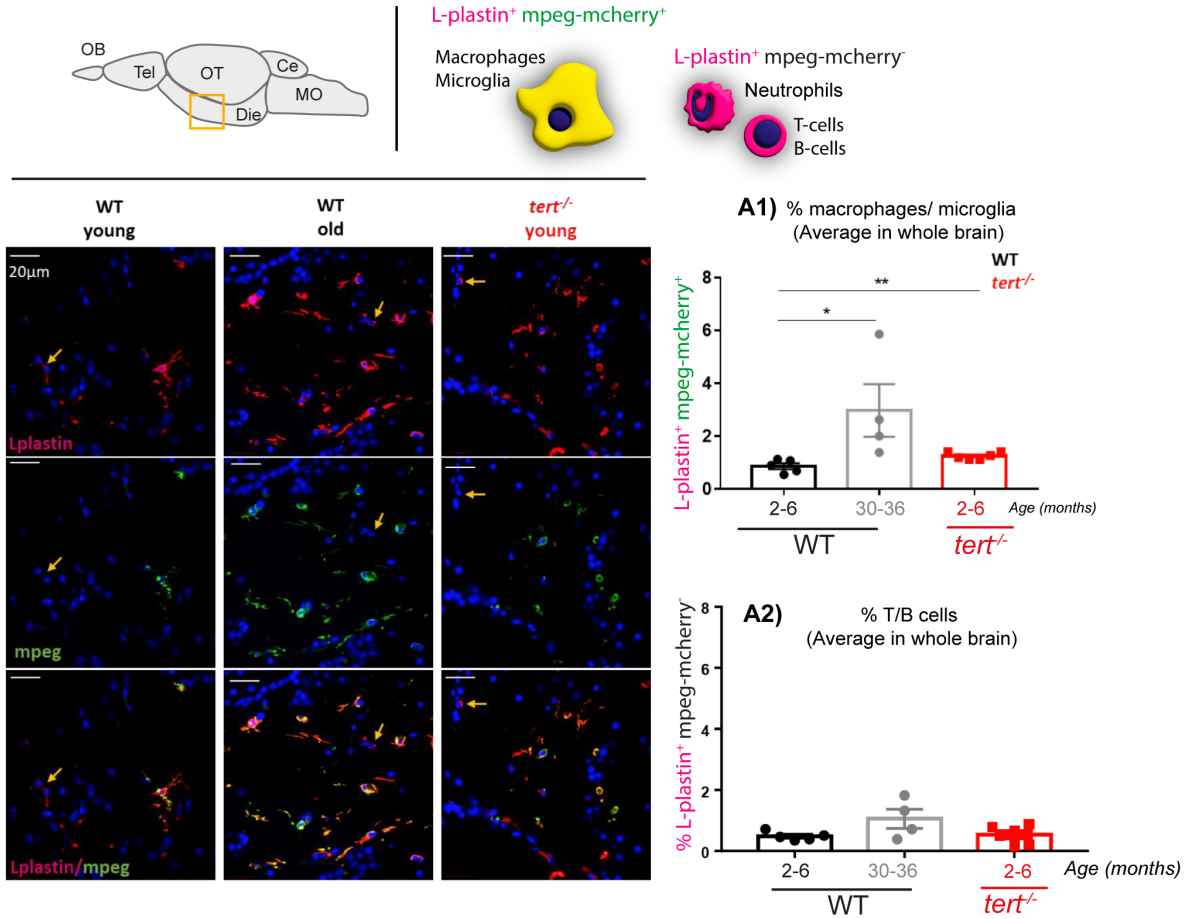

B) Chitotriosidase activity assay (marker for activated macrophages/microglia in inflammatory diseases)

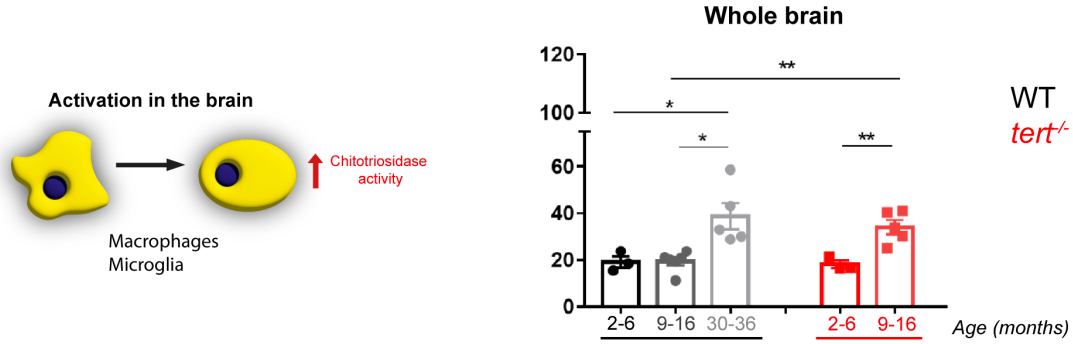

C) Correlation between senescence and immune cells

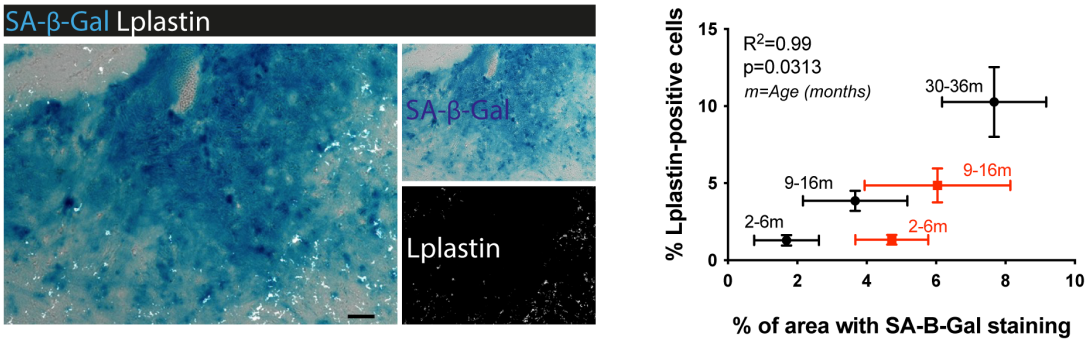

577

578 **Figure 3. Telomerase depletion is associated with increased inflammation in the aged zebrafish brain.** (A)
579 Representative images of mpeg-mcherry and L-plastin staining in the diencephalon of adult zebrafish
580 (schematic figure highlights the region imaged as diencephalon). The yellow arrows highlight Lplastin^{+}; mpeg^{-}
581 cells. (A1) Quantifications of L-plastin-positive; mpeg-positive cells (orange; from red and green co-localisation)
582 and (A2) L-plastin-positive; mpeg-negative cells (red) in the whole zebrafish brain show an increased number
583 of macrophages/microglia (L-plastin-positive; mpeg-positive cells) with natural ageing, and this is accelerated
584 in the absence of telomerase (in *tert*$^{-/-}$ at 2-6 months of age). However, we observed no differences in the
585 number of T/B cells and neutrophils (L-plastin-positive; mpeg-negative cells) with ageing, in the WT or *tert*$^{-/-}$
586 fish. N=-6 per group. (B) Schematic figure of the chitotriosidase assay (left). Quantifications (right) show that
587 chitotriosidase activity increases with natural ageing at >30 months of age, and that this is accelerated in the
588 *tert*$^{-/-}$ at the age of 9-16 months. (C) Representative images of co-staining with SA-β-Gal (blue) and L-plastin
589 (white) in brain sections show that most of the L-plastin-positive cells do not co-localise with the SA-β-Gal
590 staining (left). Staining quantification shows a significant correlation between increased number of immune
591 cells and increased expression of SA-β-Gal with ageing in both WT and *tert*$^{-/-}$ (right). (A1, A2, B) Each dot
592 represents one animal. (A1, A2, B, C) Bar errors represent the SEM. * <0.05; ** <0.01; *** <0.001.
593

594 **2.4 Telomerase (tert) depletion accelerates ageing-associated blood-brain barrier**
595 **dysfunction**

596 Because our data show that telomerase (tert) depletion accelerates ageing-associated
597 neuroinflammation (**Fig 3**) not explained by increased immune proliferation (**Supp Fig 7B**),
598 we hypothesised that there could be immune infiltration from the periphery. Immune cells
599 should not cross the Blood-brain barrier (BBB) and invade the brain in a healthy condition
600 unless the BBB is compromised (reviewed in[88]). It has been described that zebrafish have a
601 functional BBB from the 10th day post fertilisation (dpf)[89] after which molecules such as
602 horseradish peroxidase (HRP, 44,000Da), evans blue (961Da), and sodium fluorescein
603 (376Da) do not cross this barrier[89,90].
604

605 To test whether zebrafish BBB becomes leaky with ageing and whether telomerase plays a
606 role in it, we set up a BBB permeability assay in both WT and *tert*$^{-/-}$ at similar ages where
607 increased immune activation (chitotriosidase activity) was identified in the brain. To do this,
608 we performed intraperitoneal injections (IP) of an infrared fluorescent dye IRDye 680RD
609 Dextran diluted in saline (Hanks buffered solution-HBSS). We confirmed this dye's suitability
610 for assessing BBB by performing a pilot study comparing dispersion of conjugated molecules
611 of different sizes throughout the body at different time points and determined that 4kDa

612 Dextran conjugated with fluorescent dye was optimal for assessment of tissue dispersal 3
613 hrs post-injection (not shown). Three hours after injection, fish were culled, and dissected
614 brain fluorescence was measured (using a Li-cor Odyssey imaging system). Our data show
615 that BBB permeability increases with WT ageing, as measured by 4kDa dextran-FITC-
616 associated fluorescence in the brain, which was accelerated in the absence of telomerase
617 (*tert*$^{-/-}$) from the tested age of 9-16 months.
618

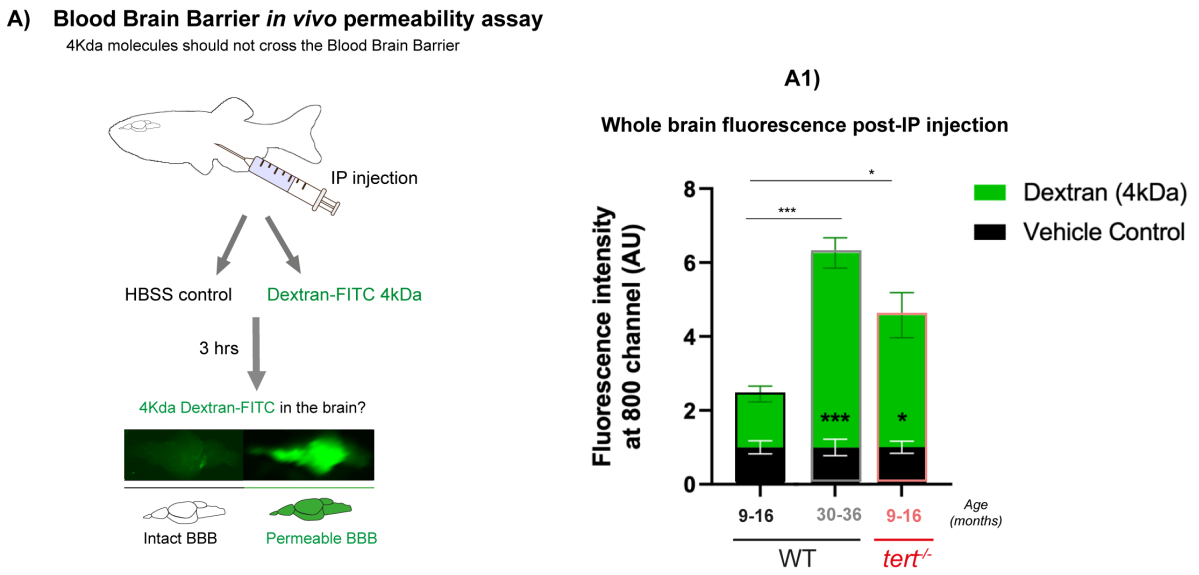

619

620 **Figure 4. Telomerase depletion is associated with increased BBB permeability with ageing in the zebrafish**
621 **brain.** (A) Schematic figure of the BBB permeability assay. Dextran-FITC 4kDa or vehicle control (HBSS) were
622 injected by intraperitoneal injection. 3 hours later the brains were dissected and imaged in the Odyssey® CLx
623 (Li-cor) to confirm the presence of Dextran-FITC. Quantification of the green fluorescence in the fish brains
624 shows higher FITC expression in old WT (>30 months) compared to middle aged ones (9-16 months). This
625 increased presence of dextran-FITC in *tert*$^{-/-}$ is already observed at 9-16 months, overall suggesting that there
626 is increased brain permeability with natural ageing and that this is anticipated in the absence of telomerase.
627 N=9-20 per group in the tested animals; N=3-6 per group in the vehicle control animals. Bar errors represent
628 the SEM. Statistics: unpaired t-tests. * $p<0.05$; ** $p<0.01$; *** $p<0.001$.
629

630 **2.5 Telomerase (tert) depletion accelerates ageing-associated behavioural changes in**
631 **zebrafish**

632 It is known that inflammation can influence behaviour. For example, lipopolysaccharide
633 (LPS)-induced peripheral inflammation has been shown to lead to behavioural alterations in
634 rodents, in a dose-dependent manner, including changes in anxiety-like behaviour[91,92]. Given

that we observed a telomerase-dependent increase in neuroinflammation with ageing, we set out to test whether it associated with any alterations in behaviour. To do this, we assessed anxiety-like behaviour using a novel tank test [93,94] in WT and *tert*$^{-/-}$ zebrafish at young and old ages (**Fig 5A**). The novel tank test showed that, with ageing, WT fish tend to spend less time in the top part of the tank, particularly at >30 months of age, indicative of increased anxiety-like behaviour. This behaviour is already detected in *tert*$^{-/-}$ at the earlier age of 9-12 months (**Fig 5B**). Importantly, no differences between groups were observed in the total distance swam throughout the test (**Fig 5C**). Therefore, the differences observed in the time spent swimming in the top area of the tank, in advanced ages, is likely to be associated to an anxiety-like behaviour phenotype rather than to potential locomotive defects. Together, lower time spent in the top part of the tank suggests reduced anxiety-like behaviour with natural ageing, which our data suggest is a telomerase-dependent phenotype of old age.

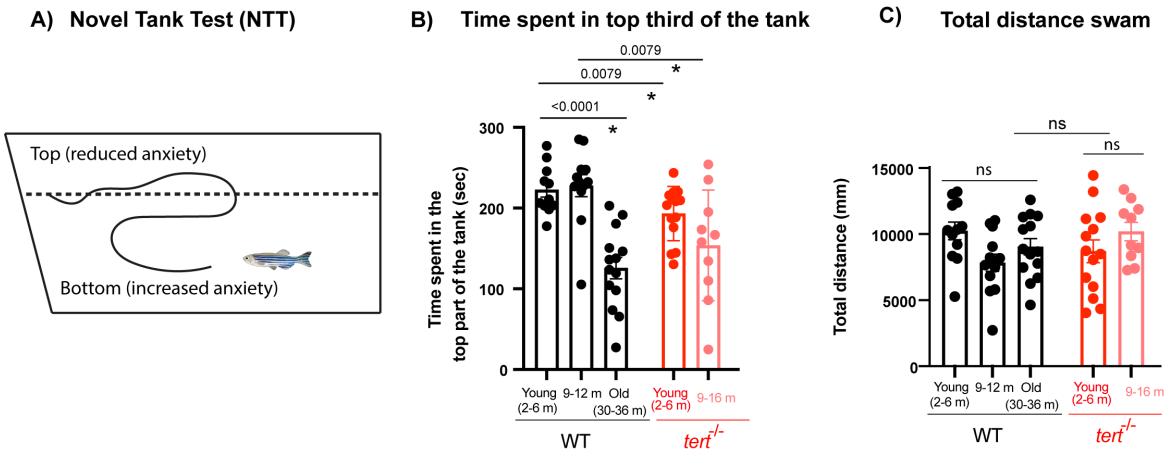

Figure 5. Telomerase depletion is associated with increased anxiety-like behaviour. (A) Schematic figure of the setup and behaviour assessment during the novel tank test (NTT). (B) Quantifications show that old WT (>30 months) spend less periods of time in the top part of the tank compared to younger siblings, and that this behaviour is already observed in *tert*$^{-/-}$ at 9-16 months. (C) Quantifications of the total distance swam during the entirety of the test show no differences between groups, suggesting that the differences observed in the time spent in the top area of the tank are not explained by a locomotive defect in advanced ages. N=10-14. Each dot represents a fish. Bar errors represent the SEM. * p<0.05; ** p<0.01; *** p<0.001.

3 DISCUSSION

660 Decreased telomerase expression, telomere shortening, senescence-associated markers and
661 inflammation have all been independently observed in the ageing brain and associated with
662 human neurodegeneration. However, causality between limited telomerase expression and
663 increased brain senescence and neuro-inflammation in a WT setting is yet to be established.
664 Here, we address these questions using the zebrafish as an ageing model which, akin to
665 humans, displays premature ageing and death in the absence of telomerase and where
666 telomere shortening is a driver of cellular senescence. We hypothesised that limited
667 expression of Tert in the aged zebrafish brain contributes to brain degeneration with ageing.
668 To our knowledge, this manuscript represents the first broad characterisation of zebrafish
669 brain ageing in the presence and absence of telomerase (Tert).
670
671 Our transcriptomic analyses highlighted increased inflammation and decreased cell cycle as
672 key signatures of ageing accelerated in the absence of telomerase (tert) which were reflected
673 at cell/tissue level and accompanied by behaviour alterations. Interestingly, some ageing-
674 associated phenotypes were accelerated from as early as 2-6 months in the *tert*$^{-/-}$, whereas
675 the majority were from 9-16 months, which led us to our current working model (Fig 6). In
676 specific, telomerase depletion accelerates ageing-associated telomere shortening,
677 accumulation of SA-β-Gal, a lysosomal protein, which are generally known to accumulate
678 with senescence; and microglia/macrophages numbers from the young age of 2-6 months in
679 *tert*$^{-/-}$.These tissue-level changes are accompanied by an increase of ageing-associated
680 increase in anxiety-like behaviour from that same early age in *tert*$^{-/-}$. Our data leads us to
681 suggests a potential model in which SA-βGAL accumulation and recruitment of immune cells.
682 Whether this increased neuroinflammation is detrimental remains to be determined, and it
683 is not entirely clear in human neurodegeneration. Neuroinflammation is associated with
684 neurodegeneration and disease in humans[50,95,96], but causality is not clear. It is not clear from
685 our data whether neuroinflammation in the aged zebrafish brain is contributing to the
686 senescence phenotypes via paracrine senescence mechanisms[87] or whether immune cells
687 are "trying" to clear senescent cells[97]. Nevertheless, even if initially recruited for clearance
688 purposes, this function may be decreased with ageing and thus chronic inflammation may
689 contribute to a senescence phenotype by increasing senescence-associated markers such as
690 SASP and DDR. Our data specifically highlights *psme2* (proteasome activator subunit 2), as a
691 particularly relevant putative SASP-associated factor, since it was identified in both our STEM

692 and broader DEGs of old age accelerated in the absence of telomerase (**Supp Fig 6**). loss of
693 proteostasis is a known hallmark of ageing and *psme2* may be involved in this crosstalk[5],
694 Potentially as a consequence of increased inflammation and accumulation of cellular
695 senescence, our data show that telomerase depletion accelerates ageing-associated
696 increase in immune activation (increased chitotriosidase activity) and BBB permeability. In
697 turn, BBB leakiness is likely to lead to further recruitment of immune cells from the
698 periphery, further exacerbating inflammation and BBB dysfunction in a positive feedback
699 loop. Of note, our broad analysis of "DEGs of old age" showed that *ctss2.1* is significantly
700 upregulated with ageing, which has recently been implicated in macrophage-driven age-
701 dependent disruption of the blood-CSF barrier [98]. BBB leakiness is likely to lead to further
702 recruitment of immune cells from the periphery potentially exacerbating inflammation and
703 BBB dysfunction in a positive feedback loop.
704
705 Together, our work suggests that telomerase has a protective role in the zebrafish brain
706 against the accumulation of senescence-associated markers and neuro-inflammation and is
707 required for BBB integrity. Importantly, the acceleration of senescence-associated markers
708 in the absence of tert occurs not only in the expected proliferative areas but also in non-
709 proliferative ones, where it is unlikely due to telomere-dependent replicative exhaustion,
710 suggesting that non-canonical roles of telomerase may be involved.

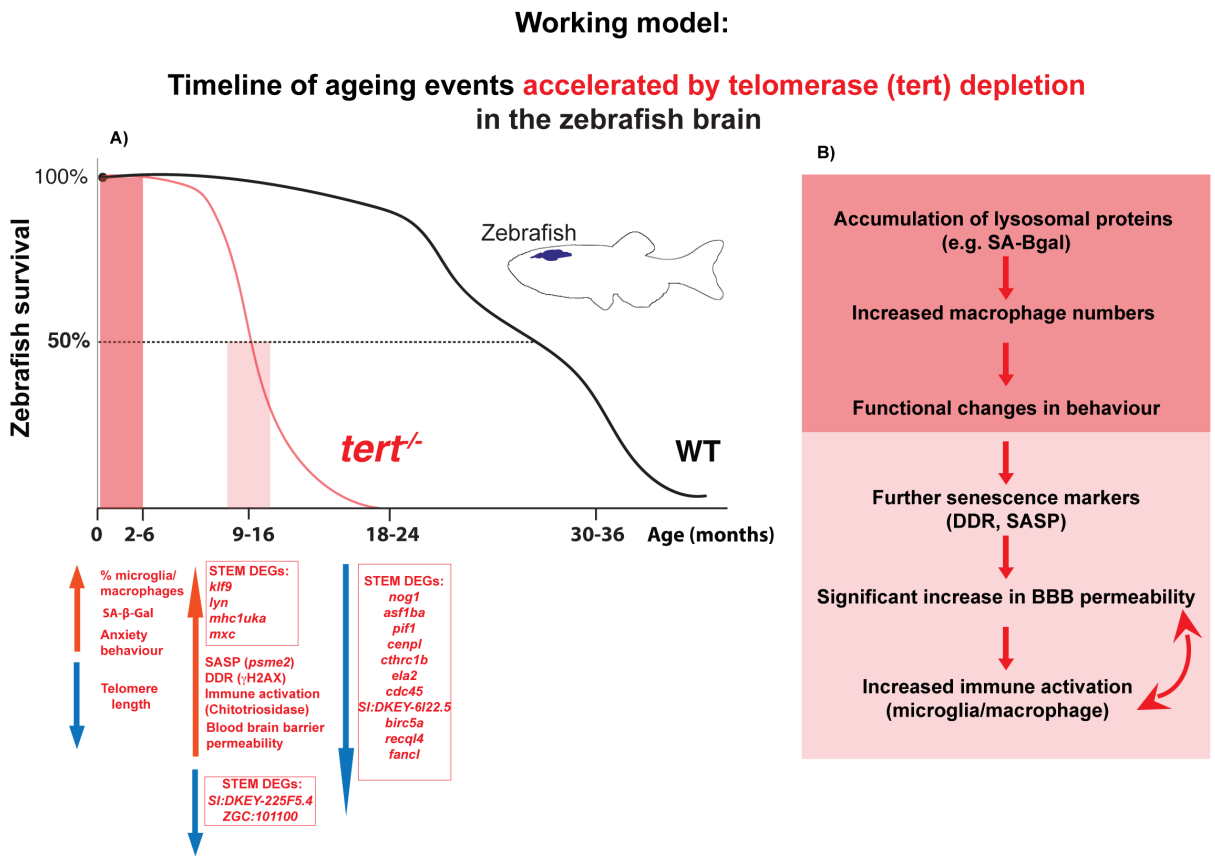

Figure 6. Working model: timeline of ageing events accelerated by telomerase depletion in the zebrafish brain. (A) Survival curve showing the early to late stages of ageing in WT fish compared to *tert*$^{-/-}$ fish, highlighting the changes we identify at cellular, tissue and functional levels with ageing and that are accelerated in the absence of telomerase, at different ages throughout their lifecourse. (B) Table summarising the sequence of events we observe in the ageing brain and that are accelerated by telomerase depletion: Accumulation of lysosomal proteins (such as SA-β-Gal), increased number of macrophages and increased anxiety-like behaviour are already observed at the young age of 2-6 in *tert*$^{-/-}$ fish (but only at later ages in WT fish). Dysfunction at lysosomes and recruitment of immune cells are likely to contribute to a senescence phenotype by increasing senescence-associated markers such as SASP and DDR, which are observed at 9-16 months in *tert*$^{-/-}$. This is accompanied by increased immune activation (increased chitotriosidase activity) and BBB permeability, at the same age, potentially as a consequence of increased inflammation and accumulation of cellular senescence. In turn, BBB leakiness is likely to lead to further recruitment of immune cells from the periphery, further exacerbating inflammation and BBB dysfunction in a positive feedback loop.

731 **4 MATERIALS AND METHODS**

732 **1. Animal husbandry, ethics, genotypes and ages**

733 Zebrafish were maintained at the standard conditions of 27-28ºC, in a 14:10 hour light-dark
734 cycle, and fed twice a day with Artemia (live rotifers) and Sparus (dry food). All the
735 experiments were performed in the University of Sheffield. All animal work was approved by
736 local animal review boards, including the Local Ethical Review Committee at the University
737 of Sheffield (performed according to the protocols of Project Licences 70/8681 and
738 PP4455093). Three strains of adult zebrafish (Danio rerio) were used for these studies: wild-
739 type (WT; AB strain), tert$^{-/\ (tertAB/hu3430)}$ and *Tg(mpeg1:mCherryCAAX)sh378* (Source:
740 University of Sheffield). Wild-type fish were obtained from the Zebrafish International
741 Resource Center (ZIRC). The telomerase mutant line tert $^{AB/hu3430}$ was generated by N-ethyl-
742 nitrosourea mutagenesis (Utrecht University, Netherlands (Wienholds et al., 2003)). It has a
743 T→A point mutation in the tert gene and is available at the ZFIN repository, ZFIN ID: ZDB-
744 GENO-100412–50, from ZIRC. The fish used in this study are direct descendants of the ones
745 used in the first studies describing this line (Carneiro et al., 2016; Henriques et al., 2013), by
746 which point it had been subsequently outcrossed five times with WT AB for clearing of
747 potential background mutations derived from the random ENU mutagenesis from which this
748 line was originated.

749

750 The tert $^{hu3430/hu3430}$ homozygous mutant is referred to in the paper as *tert*$^{-/-}$ and was
751 obtained by in-crossing our tert heterozygous AB/hu3430 strain, and WT and tert-/- fish
752 compared in this study are siblings, derived from that F1 *tert*$^{+/-}$ in-cross, following gold
753 standard guidelines to use this line, as recently reviewed here (Henriques & Ferreira,
754 2024).Similarly, in order to produce WT and *tert*$^{-/-}$ siblings carrying the
755 *Tg(mpeg1:mCherryCAAX)sh378* transgene, tert$^{+/-}$; *mpeg1:mCherryCAAX* were incrossed.
756 In this study, we used only males, given that the kinetics of telomerase-dependent ageing in
757 zebrafish has been well described for males only[18,20], which is a limitation of the model and
758 this study. Nevertheless, there is data showing "Limited sex-biased neural gene expression
759 patterns across strains in Zebrafish"[99], giving strength to our study.

760

761 Genotyping was performed by PCR of the tert gene as before. To study age-related
762 phenotypes in the zebrafish brain, we used 30-36 months old fish for what we consider old

763 in WT (in the last 25-30% of their lifespan), and we considered the *tert*$^{-/-}$ old fish at the
764 equivalent age (18-24 months), which approximately corresponds to the last 25-30% of their
765 lifespan. In specific, 'Old' was defined as the age at which most of the fish present age-
766 associated phenotypes, such as cachexia, loss of body mass and curvature of the spine. These
767 phenotypes develop close to the time of death and are observed at 30-36 months of age in
768 WT and at >18-24 months in *tert*$^{-/-}$ [18,20].
769
770 **Note on Zebrafish gene and protein nomenclature**
771 This manuscript followed the agreed convention as described in:
772 *https://zfin.atlassian.net/wiki/spaces/general/pages/1818394635/ZFIN+Zebrafish+Nomenc*
773 *lature+Conventions*
774
775 **In summary:**
776 **Gene nomenclature**
777 Genes should be named after the mammalian orthologue whenever possible. When
778 mammalian orthologues are known, the same name and abbreviation should be used,
779 except all letters are italicized and lower case. Members of a gene family are sequentially
780 numbered.
781 **Examples:**
782 Names - engrailed 1a, engrailed 2b
783 Symbols - eng1a, eng2b
784 **Protein nomenclature**
785 The protein symbol is the same as the gene symbol, but non-italic and the first letter is
786 uppercase.
787 Note the differences between zebrafish and mammalian naming conventions:
788 **species / gene / protein**
789 zebrafish /*shha*/ Shha
790 human / *SHH* / SHH
791 mouse / *Shh* / SHH
792
793 **2. Tissue fixation**

794 Paraffin-embedded sections: Fish were culled by immersion in concentrated tricaine (MS-
795 222). After terminal anaesthesia, the animals were fixed by immersion in 50 ml of Neutral
796 buffered formalin (NBT, VWR International, Radnor, PA, USA) at 4ºC for 48h-72h and
797 decalcified in 50 ml of 0.5M ethylenediaminetetraacetic acid (EDTA), pH 8, for additional 48-
798 72h. Then, the whole fish were paraffin-embedded (in formalin I for 10min, formalin II for
799 50min, ethanol 50% for 1h, ethanol 70% for 1h, ethanol 95% for 1h 30min, ethanol 100% for
800 2h, ethanol 100% for 2h 30min, 50%:50% of ethanol 100% : Xilol for 1h 30min, xylene I for
801 3h, Xylene II for 3h, paraffin I for 3h, paraffin II for 4.30h), longitudinally sliced (sagittal slices,
802 3 µm thick, using the Leica TP 1020) and stored at room temperature (RT). To do this, diluted
803 ethanol absolute (VWR International) and paraffin histosec pastilles (Merck & Co,
804 Kenilworth, NJ, USA) were used.
805
806 Cryosections: Fish were culled by immersion in concentrated MS-222, followed by
807 immediate decapitation (Schedule 1 method). The brain was dissected, transferred to and
808 rinsed in cold L15 (Thermo Fisher Scientific, Waltham, MA, USA). Afterwards, the brain was
809 fixed in 4ml NBT overnight at 4°C, washed in 3ml cold Phosphate Buffered Saline (PBS, 1x),
810 and immersed in 4ml of 30% sucrose in PBS overnight at 4ºC for cryoprotection. Finally, the
811 tissue was mounted in a base mould (Electron Microscopy Sciences, Hatfield, PA, USA), with
812 O.C.T. (VWR), snap frozen, and stored at -20°C. Prior to use, 13µm coronal tissue sections
813 were cut using a Leica CM1860 cryostat, attached to SuperfrostPlus slides (Epredia) and air
814 dried for a minimum of 2h at RT. Slides were stored at -20ºC for a maximum of 3 months.
815
816 **3. RNA probe synthesis for *in situ* hybridisation (ISH)**
817
818 A Zebrafish p16-like fragment was amplified using the following primers: FW
819 cgttgaacATGAACGTCG and REV tctttaaacattTTAAACACGATTGAG and cloned into the pCR-
820 Blunt ii- TOPO vector (Thermofisher Scientific Inc, USA), For anti-sense probe generation, the
821 plasmid was linearised with HindIII (New England Biolabs) and synthesis carried out with T7
822 RNA polymerase (New England Biolabs) and DIG-labelling mix (Merck Life Science UK
823 Limited).
824 For the sense probe, plasmid was linearisated with XhoI (New England Biolabs), and probe
825 synthesised with SP6 RNA polymerase (New England Biolabs).

826 Probes were cleaned up using SigmaSpin post-reaction clean-up columns (Sigma Aldrich)
827 and used at a final concentration of 3ng/µl for hybridisation.
828
829 **4. Chromogenic RNA fluorescence *in situ* hybridisation (RNA-FISH)**
830 Cryosections were fixed with NBT for 10min at RT followed by 3x washes with Diethyl
831 pyrocarbonate (DEPC)-treated PBS. Sections were then acetylated with 11.2 µl
832 triethanolamine and 2.5 µl acetic anhydride per 1ml H_2O for 10 min at RT (both Sigma
833 Aldrich). After 3x washes in DEPC-PBS, sections were incubated in prehybridization solution
834 (prehyb) and coverslipped (prehyb: 50% formamide, 5x SSC pH7, 2% Blocking reagent, 0.1%
835 TritonX100, 0.5% CHAPS, 1mg/ml yeast RNA, 50 µg/ml heparin sodium salt (all from Sigma
836 Aldrich)) for 1h at 68°C in a humidified box. The solution was replaced with 200µl l fresh
837 prehyb containing 3ng/ µl DIG-labelled RNA probe, coverslipped and incubated overnight at
838 68°C in a humidified box.
839 Following this, coverslips were removed and slides were washed for 1h in prewarmed wash
840 #1 (50% formamide, 5xSSC pH4.5, 1%SDS) at 68°C, then 1h in prewarmed wash #2 (50%
841 formamide, 2xSSCpH4.5, 1% Tween20) at 68°C in coplin jars.
842 Slides were washed in TBS-T (8g NaCl, 0.2g KCl, 25ml 1M Tris pH7.5, 10ml tween20 per L
843 solution) at RT, blocked in TBS-T/10% Heat inactivated goat serum for 40 min at RT, then
844 incubated in fresh block/alkaline phosphatase-conjugated anti-DIG at 1:2000 for 80min at
845 RT.
846 Slides were washed extensively in TBS-T followed by 3x washes in freshly prepared NTMT
847 (for 50ml solution:1ml 5M NaCl, 2.5ml 2M Tris pH9.5, 2.5ml 1M MgCl2, 500ul Tween20,
848 43.5ml ddH2O). Development was started by incubation in filtered staining solution ((4.5ul
849 NBT +3.5ul BCIP per 1ml NTMT (both Merck Life Science UK Limited)) at RT in the dark.
850 Development was monitored daily with replenishment of fresh filtered staining solution.
851 Once the signal was clear, with minimal background staining, the reaction was stopped by
852 washing in PBS. Slides were mounted in glycergel (Agilent, Santa Clara, CA, USA) or
853 vectashield (2BScientific) before imaging on a Nikon Ti inverted microscope at 10x. Images
854 were tiled using Nikon elements software. For analysis, the diencephalon and optic tectum
855 (including PGZ) were delineated and thresholded using fiji image J to determine the area of
856 positive staining within each macroarea. The percentage of positive tissue per section
857 macroarea was then determined.

858

859 **5. Immunofluorescence (IF)**

860 Paraffin sections with whole fish slices were dewaxed and hydrated through the following
861 sequence of washes: histoclear (Scientific Laboratory Supplies, Wilford, Nottingham, UK, 2x5
862 min), 100% ethanol (Thermo Fisher Scientific, 2x5 min), 90% ethanol (5 min), 70% ethanol (5
863 min), and distilled water (2x5 min). Cryosections were hydrated in PBS for 10 min before
864 proceeding. After antigen retrieval in 0.01M citrate buffer at pH 6.0 (sub-boiling at 800 W in
865 a microwave for 10 min), the tissue sections were permeabilized in PBS 0.5% Triton X-100
866 (for 10 min) and blocked in 3% bovine serum albumin (BSA), 5% Goat Serum in 0.3% Tween-
867 20 in PBS (for 1 h). Then, primary antibody incubation (overnight at 4ºC) was followed by
868 washes in PBS 0.1% Tween-20 and secondary antibody incubation (1 h at RT or overnight at
869 4ºC). Finally, the tissues were incubated in DAPI for nuclear staining (Thermo Fisher
870 Scientific), 1:10,000 dilution in PBS from a 10mg/ml stock, for 10 min; washed in PBS 1x,
871 mounted with vectashield (Vector Laboratories, Burlingame, CA, USA), covered with a
872 coverslip (Scientific Laboratory Supplies), and sealed with clear nail varnish. For details on
873 the primary and secondary antibodies refer to Table 1 and Table 2, respectively.

874

875 **6. Telomere-fluorescence *in situ* hybridization (telo-FISH)**

876 Telo-FISH was performed after IF. Briefly, after incubation with the secondary antibody and
877 respective washes, the tissues were fixed in 4% PFA (SIGMA-ALDRICH) for 20min. Washes in
878 PBS, 3x 10min were followed by a dehydration step consisting of washes with ice cold 70%,
879 90% and 100% ethanol (Thermo Fisher Scientific, 3min each). After this, the slides were left
880 to dry for 1h, 10µl of hybridisation solution was pipetted on top of each tissue section and
881 the slides were covered with a coverslip. Hybridisation solution (for a total volume of 100µl):
882 8.56µl MgCl2 buffer pH 7.0, and 82mM sodium hydrogen phosphate (SIGMA-ALDRICH), 70µl
883 of deionised formamide (Thermo Fisher Scientific), 1µl of 1mM Tris, pH 7.5 (SIGMA-
884 ALDRICH), 5µl of 1x blocking buffer (10x blocking reagent (Merck & Co.) diluted to 1x in
885 maleic acid (SIGMA-ALDRICH)), 2µl of PNA probe (Telo-Cy3, zebrafish, 568; Cambridge
886 Research Biochemicals, Cleveland, UK), 2µl of Cent-Fam probe (488; Eurogentec, Liège,
887 Belgium), and 11.44µl of dH2O.

888

889 The slides were incubated for 10min at 80°C for DNA denaturation, followed by incubation
890 for 2h at RT, in the dark, to allow the probe to hybridise with the complementary DNA. After
891 the incubation period, coverslips were gently removed and the slides were washed for 10min
892 in a solution made of 70% formamide (SIGMA-ALDRICH), 10% 2x saline-sodium citrate (SSC,
893 SIGMA-ALDRICH) and 20% dH2O. This was followed by two more washes (10min each), in 2x
894 SSC. SSC was diluted from a 20x stock solution consisting of 88.3g of Tri- sodium citrate
895 dihydrate (SIGMA-ALDRICH) and 175.3g of NaCl (SIGMA-ALDRICH), diluted in dH2O to a total
896 volume of 1L, adjusted to pH of 7.0 and autoclaved. Finally, the slides were washed in PBS,
897 incubated in DAPI (Thermo Fisher Scientific) for 10min and mounted as previously described
898 in section 2.3.2.
899
900 **7. IF and telo-FISH imaging and quantification**
901 IF and telo-FISH staining was imaged using the DeltaVision microscope, Nikon Widefield
902 inverted microscope or a Nikon Ti2 W1 spinning disc confocal at the Wolfson Light
903 Microscopy Facility (LMF), using a 40x objective. An average of 20 images were acquired from
904 the brain of each animal (paraffin sections) for longitudinal paraffin sections and 18 for
905 transverse cryosections (minimum 6 images per macro-area). For images showing whole
906 brain transverse cryosections, either 4x or 10x images were taken, with tiling in Nikon
907 elements software for the latter. Imaging settings were kept consistent within experiments
908 for accurate comparisons.
909 After acquisition, the images were analysed by manual counting: (1) the number of cells with
910 more than 5 foci of γH2AX (considered γH2AX+ cells) PCNA-, (2) the number of PCNA+ cells,
911 (3) the number of L-plastin^{+}, (4) the number of mpeg^{+} cells, and (5) the total number of cells.
912 Telo-FISH staining was quantified by the intensity of the mean of the nucleus. The ratio
913 'telomeres/centromeres' was calculated by dividing the intensity of the mean of telomeres
914 (568 channel) by the intensity of the mean of centromeres (488 channel), which normalises
915 the telomeric probe signal by the centromeric probe signal within individual cells. The brain
916 commonly exhibits cytoplasmic autofluorescence from vascular and other cell types. These
917 were excluded from our analyses by comparison to neighbouring control sections stained
918 only with secondary antibodies. Nuclear markers such as γH2AX, PCNA were only classed as
919 positive when they showed signal in the nucleus as determined by co-labelling with DAPI.
920 For telomeric and centromeric labelling analysis, individual nuclei were circumscribed based

921 on DAPI labelling and mean gray fluorescence determined. Mpeg$^+$ and Lplastin$^+$ cells were
922 manually counted and could be easily distinguished from autofluorescent cells based on
923 strength of signal and morphology.
924 The analysis was performed on raw images, using the ImageJ Fiji (v. 1.51). Images were then
925 processed with Abode Illustrator 21.0.2 for display purposes.
926
927 Table 1. Primary antibodies used for immunostaining.

Antibody, species, and type	Dilution factor	Catalogue number; company; country
PCNA mouse monoclonal	1:500	NB500-106; Novus Biologicals, Littleton, CO, USA
γH2AX, rabbit polyclonal	1:500	GTX127342; GeneTex, Irvine, CA, USA
L-plastin (Lcp1), rabbit polyclonal	1:200	GTX124420; Novus Biologicals, Littleton, CO, USA
RFP, mouse monoclonal	1:500	GTX82561; GeneTex, Irvine, CA, USA

928
929 Table 2. Secondary antibodies used for immunostaining.

Antibody, species, and type	Dilution factor	Catalogue number; company; country
Goat anti-rabbit IgG Alexa Fluor® 488	1:500	A11008; Invitrogen, Carlsbad, CA, USA
Goat anti-rabbit IgG Alexa Fluor® 568	1:500	10032302; Thermo Fisher Scientific, Waltham, MA, USA
Goat anti-mouse IgG Alexa Fluor® 647	1:500	A21235; Thermo Fisher Scientific, Waltham, MA, USA

930
931 **8. SA-β-Gal**
932 The Senescence-Associated β-Galactosidase Staining Kit (Cell Signalling Technology, Danvers,
933 MA, USA) was used to perform the SA-β-Gal staining, following manufacturer's instructions.

934 Whole brain SA-β-Gal staining: Fish were culled with neat Tricaine and decapitated. Whole
935 heads were fixed in 4ml PFA overnight at 4c with shaking. The following day, whole heads
936 were washed 3 x for 1h in PBS at RT with slow shaking. Whole brains were then dissected in
937 fresh PBS and immersed in 2ml in SA-β-Gal staining solution mix, consisting in 1x staining
938 solution (pH 5.9), 1x solution A, 1x Solution B, 1mg/ml Xgal (SA-β-Gal staining kit #9860 by
939 Cell Signaling Technology). and incubated at 37°C overnight with slow shaking in the dark.
940 The following day, brains were washed 3 x for 1h in PBS at RT with slow shaking and imaged
941 using a Nikon SMZ1500 Stereomicroscope (2000).
942 .
943 SA-β-Gal staining on cryosections: Briefly, after rinsing the cryosections in 1x PBS for 5 min,
944 200ul of β-Gal staining solution was added per slide as above. Then, the slides were
945 coverslipped and incubated at 37ºC overnight in a humidified chamber box. The following
946 day, cryosections were rinsed in 1x PBS (3x1min), and mounted in glycergel (Agilent, Santa
947 Clara, CA, USA). Slides were then imaged using an Olympus BX60 microscope or Nikon Ti
948 inverted microscope at 10x with tiling using Nikon elements software.
949 Image analysis was done using ImageJ Fiji as described for RNA-FISH. Images were then
950 processed with Abode Illustrator 21.0.2 for display purposes.
951
952 For SA-β-Gal combined with IF, sections were first labelled with SA-β-Gal as described above,
953 then fixed for 10min with NBT at RT, rinsed and processed for IF as described in methods
954 section 5 .
955
956 **9. RNA Extraction**
957 Fish were culled by Schedule 1 method (as described before in section 2.2). Zebrafish brains
958 were dissected, transferred to a microcentrifuge tube with 100 µl of Trizol (Thermo Fisher
959 Scientific), snap frozen in dry ice and stored at -80ºC until RNA extraction.
960 For RNA extraction, the tissue was homogenised with a mechanical homogenizer (VWR
961 International) and 1.5 pestle (Kimble Chase, Vineland, NJ, USA), and an extra 50 µl of fresh
962 Trizol (Thermo Fisher Scientific) was added. After 5 min of incubation at RT, 30 µl of
963 chloroform (1:5, VWR International) was added. The samples were then incubated for
964 further 3 min at RT and centrifuged (at 13,000g for 30 min at 4ºC). The resulting upper
965 aqueous phase was transferred to a new microcentrifuge tube, and isopropanol (Thermo

966 Fisher Scientific) was added (approximately 83% of the amount of aqueous phase). After an
967 incubation of 10 min at RT, the samples were centrifuged (13,000g for 15 min at 4ºC) and
968 the supernatant was discarded. The pellets were washed in 250 µl of 75% ethanol twice and
969 then left to air dry. In the end, the pellets were resuspended in 14 µl of nuclease-free water
970 (VWR International) and stored at -80ºC. All the samples were analysed by Nanodrop 1000
971 Spectrophotometer to measure the concentration of RNA. Some samples (randomly chosen)
972 were also analysed in the Bioanalyzer to assess RNA integrity. All the samples included in this
973 study had an RNA integrity number (RIN) of >9.
974
975 **10. RNA sequencing**
976 RNA-Sequencing was performed at the Genomics and Sequencing facility of Sheffield
977 Institute for Translational Neuroscience (SITraN). Mature RNA was isolated and fragmented
978 using the NEBNext Poly(A) mRNA Magnetic Isolation Module (New England Biolabs Inc),
979 following manufacturer's instructions. The libraries were prepared using the NEBNext Ultra
980 Directional RNA Library Prep Kit (Illumina), following manufacturer's instructions. The
981 NEBNext Multiplex Oligos from Illumina (Index Primers Set 1, New England Biolabs Inc) was
982 used for the library preparation using the following PCR program: 98ºC for 30 sec (1 cycle),
983 98ºC for 10 sec followed by 65ºC for 75 sec (8 cycles), and 65ºC for 5min. The PCR product
984 (≈50µl) was then purified using 45µl of Oligo dT Beads (Agencourt AMPure XP), followed by
985 three washes with ethanol 80%. After air-drying, the dscDNA was eluted by adding 23µl of
986 0.1x TE, and the resulting 20µl of the library were collected. Sequencing was run on an
987 Illumina HiScan SQ sequencer, using a high output run and sequencing by synthesis V3
988 chemistry on a single 100 base pair (bp) run. The sequencing process was monitored in real-
989 time using Sequencing Analysis Viewer v1.8.37 Software, and therefore quality control was
990 performed during and after sequencing. Then, the data was imported into a FASTA file
991 format to perform the analysis.
992
993 **11. RNA Sequencing analysis**
994 <u>Data processing:</u>
995 Featurecounts was run to obtain per-gene read counts. We calculated the transcriptome
996 coverage for each sample, defined as the number of unique sequencing reads aligning to
997 annotated transcriptomic regions. Coverage was estimated by multiplying the number of

998 assigned reads (as determined by featureCounts) by the read length and dividing by the
999 estimated total transcriptome length of approximately 76 Mb (from the Ensembl
1000 GRCz11_109 GTF file). On average, we obtained a coverage of 12X across all samples,
1001 corresponding to an average assignment rate of approximately 65%."
1002
1003 Differential expression: To identify signatures of ageing, WT brain samples were subjected
1004 separately to DESEq2 analysis, comparing the time points 9, 22 and >30 months with the
1005 time-point of 2 months. Then, *tert*$^{-/-}$ samples at 2, 9 and 22 months were compared with WT
1006 at 2 months, to identify telomerase-dependent ageing processes.
1007 Enrichment analysis: Pathway enrichment analysis was performed using the Functional
1008 Annotation Bioinformatics Microarray Analysis programme (https://david.ncifcrf.gov/).
1009 Pathways identified in both Gene Ontology Biological Process (GO-BP) and KEGG databases
1010 were included in the analysis. The top 10 GO-BP and KEGG terms were then plotted into a
1011 heatmap using graphpad Prism.
1012 Hypergeometric enrichment analysis:
1013 To assess whether the genes identified through the STEM analysis were over-represented in
1014 specific brain cell types, we performed over-representation analysis using Fisher's Exact Test
1015 under the hypergeometric distribution. For each cell type from the previously published
1016 adult zebrafish brain single-cell RNA-seq dataset [65] , we used the authors' defined gene
1017 programmes, consisting of marker genes with adjusted p-values < 0.05. These marker genes
1018 were compared to the list of STEM analysis genes to test whether the overlap was greater
1019 than expected by chance, relative to the total number of protein-coding genes in the
1020 zebrafish genome. A Fisher's Exact Test was applied for each cell type and resulting p-values
1021 were adjusted for multiple comparisons using the Bonferroni correction method.
1022 Mapping to the hallmarks of ageing: We analysed the recent Frenk & Houseley's paper[67],
1023 which describes the different transcriptional hallmarks of aging. In this paper, the different
1024 hallmarks are defined within specific text sections. For each hallmark, we collected groups
1025 of keywords that could be within GO term names. The complete list of GO term names was
1026 extracted from the file go-basic.obo from the Gene Ontology website
1027 (https://geneontology.org/). We then established lists of GO term names for each
1028 transcriptional hallmark of aging. The mapping table between the hallmarks, the keywords,
1029 and the lists of GO term names is available in the table GO_to_HA-THA_V1.csv.

1030

1031 Zebrafish genes and their associated GO term names were retrieved from the mapping
1032 function Gene2GoReader() from the Python library goatools. We built 3 distinct dictionaries
1033 for each GO category (Biological Process, Molecular Function, and Cellular Component),
1034 where the entrezgene IDs are associated with their GO term names. From the differential
1035 analyses, we obtained different lists of gene symbols that must first be mapped to
1036 entrezgene ID, using the Python library mygene. Each gene ID is associated with a list of GO
1037 term names. To assess a particular transcriptional hallmark of aging to a given gene, we
1038 parsed their associated list of GO term names and mapped them to their corresponding
1039 hallmark of aging.

1040

1041 Depending on the situation, the attribution of the hallmark of ageing is done as follows: 1)
1042 all the GO term names are mapped to the same transcriptional hallmark of ageing, 2) the GO
1043 term names are mapped to several transcriptional hallmarks of ageing, the hallmark with the
1044 highest number of occurrences is chosen. Otherwise, the gene is assigned with an
1045 "ambiguous" hallmark of ageing if 3) none of the GO term names are mapped to any
1046 transcriptional hallmarks of ageing, then the gene is not annotated with a transcriptional
1047 hallmark of aging.

1048

1049 **12. cDNA synthesis for Real-time qPCR**

1050

1051 cDNA synthesis was performed using the the SuperScript II RT Kit (Thermo Fisher Scientific,
1052 USA) kit, following manufacturer's instructions. Approximately 300ng of each RNA sample
1053 was mixed with 0.5 µL of 500 µg/mL random primers, 1 µL 10 mM dNTPs, and sterile, PCR-
1054 grade water to a final volume of 12 µL. Samples were heated to 65 °C for 5 minutes, followed
1055 by cooling at 4 °C and placement on ice. To each sample, 4 µL First-Strand Buffer, 2 µL 0.1 M
1056 DTT, and 1 µL NxGen RNase inhibitor (LGC Biosearch Technologies, Hoddesdon, UK) were
1057 added and gently mixed. Samples were heated to 25 °C for 2 minutes, followed by the
1058 addition of 1 µL SuperScript™ II RT. Samples were then incubated at 25 °C for 10 minutes,
1059 followed by incubation at 42 °C for 50 minutes, before the reaction was inactivated by
1060 heating at 70 °C for 15 minutes.

1061

1062 Real-time qPCR

1063 cDNA samples from zebrafish brains were analysed by real-time qPCR using SsoAdvanced
1064 Universal SYBR Green Supermix (Bio-Rad), forward and reverse primers at a final
1065 concentration of 200 nM (Table 1), and cDNA diluted 1:40. Samples were analysed in
1066 triplicate. The CFX384 Touch Real-Time PCR Detection System (Bio-Rad) was used to run each
1067 real-time qPCR. The program settings were: 95 °C for 30 seconds, followed by 40 cycles of
1068 95 °C for 5 seconds and 58.4 °C for 15 seconds. A melt curve analysis was included in each
1069 experiment by increasing the temperature from 65 °C to 95 °C at a 0.5 °C/ 5 second
1070 increment. To ensure that the Cq values of the sample cDNA fell within a linear range in
1071 which the primer efficiency was between 90-110%, a two-fold serial dilution of pooled cDNA
1072 from randomly selected samples were included in each run, with curves containing at least
1073 5 data points. No template (water) and no reverse transcriptase controls were also included
1074 in each run.

1075

1076 During analysis, the standard error of each triplicate was calculated and samples with
1077 triplicates presenting a standard deviation ≥0.5 were excluded. The fold change expression
1078 for each gene was calculated using the ΔΔCt method [1]. Expression of each target gene was
1079 normalised to the housekeeper gene (*beta-actin*) and the average fold-change in values for
1080 each group compared to the young WT group was calculated.
1081 Graphs and respective statistical analysis were performed using GraphPad Prism 10.4.2.
1082 Normality was assessed using the Shapiro-Wilk test and statistical comparisons carried out
1083 using a two-way ANOVA, followed by Dunnett's test for multiple comparisons. A p-value of
1084 <0.05 was considered significant.

1085

1086 **13. Protein extraction and quantification**

1087 Fish were culled by Schedule 1 method as previously described. Brain tissue was dissected,
1088 transferred to a microcentrifuge tube and immediately snap-frozen in liquid nitrogen. The
1089 samples were stored at -80°C until protein extraction.
1090 The tissue was homogenised in 100µl of ultra-pure water using a mechanical homogenizer
1091 (VWR International) and RNAse-free disposable pestles (Thermo Fisher Scientific) for

1092 approximately 30sec, on ice. Then, the samples were spun down at 4°C, at 2,000rpm, for
1093 5min. After transferring the supernatant to a new tube, samples were stored at -80°C until
1094 further use.
1095
1096 Protein extracts were quantified by the bicinchoninic acid (BCA) method, using the Pierce™
1097 BCA Protein Assay Kit (Thermo Fisher Scientific), following manufacturer's instructions.
1098 Briefly, a standard curve was prepared with a range of 0.2-2µm of BSA, along with a blank
1099 control (containing ultra-pure water only). A total of 5µl of each protein extract was mixed
1100 with 1ml of BCA, in microcentrifugation tubes, and incubated at 37°C for 10min in a water
1101 bath. After adding an additional 20µl of copper sulphate, the solution was mixed and
1102 incubated at 37°C for 20min. Then, 200µl of each sample (or BSA standard curve) were
1103 transferred to a Corning™ Costar™ Brand 96-Well EIA/RIA Plate (Thermo Fisher Scientific), in
1104 duplicates, and absorbances were read in a Varioskan Plate Reader at a wavelength of
1105 562nm.
1106
1107 **14. Chitotriosidase activity assay**
1108 Chitotriosidase activity was measured using the protocol previously described by[100]. This
1109 method allows assessment of the hydrolysis capacity of 4–methylumbelliferyl–β-D-N, N', N"-
1110 triacetylchitotriose (4-MU-chitotrioside), by chitotriosidase enzyme.
1111
1112 Briefly, a total of 10µl of protein extract per sample was mixed with 100µl of substrate
1113 solution and incubated at 28°C for 6 min. A blank control containing 10µl of ultra-pure water
1114 was prepared alongside the samples. Substrate solution consisted in 4-MU-chitotrioside
1115 (SIGMA-ALDRICH) diluted in McIlvaine solution at pH 5.2 (1.73mg of 4-MU-chitotrioside per
1116 100 ml of McIlvaine solution). To make the McIlvaine solution, stock solutions of 0.1M citric
1117 acid (SIGMA-ALDRICH) and 0.2M di-sodium hydrogen phosphate (SIGMA-ALDRICH) were
1118 mixed at a ratio of 45% and 55%, respectively, obtaining a final pH of 5.2. After incubation,
1119 1ml of stop solution (0.25M glycine buffer, pH 10.4, containing 0.01% Triton X-100 (SIGMA-
1120 ALDRICH) was added to each sample (and blank control), and 200µl of the final solution was
1121 transferred to a Corning™ Costar™ Brand 96-Well EIA/RIA Plate (Thermo Fisher Scientific).
1122 Duplicates of each sample were used. An extra microcentrifuge tube was prepared with
1123 200µl of standard solution (5µm 1,4-Methylumbelliferone, SIGMA-ALDRICH) and 900µl of

1124 stop solution. A volume of 200µl of the final solution was transferred to the 96-well plate, in
1125 duplicates. The fluorescence was then read in a Varioskan Plate Reader (excitation: 365nm;
1126 emission: 450nm). Finally, the chitotriosidase activity was calculated in nM/h/ml, using
1127 Formula 4.
1128
1129 **T**, fluorescence of test samples
1130 **B**, fluorescence of blank
1131 **Std**, standard

1132 $$\frac{(T-B)}{std} x \frac{60}{incubation\ time\ [min]} x \frac{1000}{volume\ [\mu l]}$$

1133
1134 **15. Blood Brain Barrier (BBB) permeability assay**
1135 To test BBB permeability, a total of 5µl of 0.1% IRDye 680RD Dextran (LI-COR Biosciences,
1136 Lincoln, NE, USA) diluted in HBSS (Thermo Fisher Scientific) were injected by intraperitoneal
1137 injection (IP). Two different sizes of the compound were tested, with the following molecular
1138 weights: 4kDa and 70kDa. A group of fish injected with 5µl of HBSS alone was used as a
1139 vehicle control group. The fish were culled 3h after IP, and the brains were collected and
1140 imaged using a LI-COR Odyssey CLx machine (LI-COR). The brain fluorescence was then
1141 quantified using the Image Studio 4.0 Software for Odyssey CLx (LI-COR).
1142
1143 **16. Mitochondrial complex assays**
1144 Homogenised brain tissue was diluted to approximately 0.7mg protein/ml and subjected to
1145 3 cycles of rapid freeze-thawing in liquid nitrogen. All spectrophotometric assays were
1146 performed at 28°C in 200µl final volume using a Fluostar Omega plate reader. For assessing
1147 complex I activity, the assay buffer was 25mM KH_2PO_4, 5mM $MgCl_2$, (pH7.2), 3mM KCN,
1148 2.5mg/ml BSA, 50µM ubiquinone, 2µg/ml antimycin A. Complex I activity was determined by
1149 measuring the oxidation of nicotinamide adenine dinucleotide reduced disodium salt
1150 (NADH) at 340nm with a reference wavelength of 425nm (ε = 6.22mM^{-1} cm^{-1}). 125µM NADH
1151 started the reaction, and 3µg/ml rotenone was used to inhibit the reaction. For assessing
1152 Complex II activity, the brain homogenate was incubated for 10min in assay buffer containing
1153 25mM KH_2PO_4, 5mM $MgCl_2$, (pH 7.2), 3mM KCN, 20 mM succinate. 50µM 2,6-DCPIP, 2µg/ml
1154 antimycin A and 3µg/ml rotenone were then added, and baseline measurements recorded.

1155 The reaction was started with the addition of 50µM ubiquinone Q1 and complex II activity
1156 determined by measuring the reduction of 2,6-dichlorobenzenone-indophenol sodium salt
1157 (2,6-DCPIP) at 600nm (ε = 19.2mM^{-1} cm^{-1}). Complex I and complex II activity rates are
1158 normalised to citrate synthase activity.
1159

1160 **17. Novel tank diving test (NT)**

1161 The novel tank diving test (NT) was performed as previously reported by [93] and[94]. Briefly, 6
1162 T-75 transparent flasks filled with aquarium water were inserted in the Zantiks LT
1163 behavioural unit (Zantiks ltd, Cambridge, UK). After 1h acclimatisation period in the
1164 behaviour room, the fish were individually placed into the flasks and allowed to free swim
1165 for 5 min. A side camera was used to record the behaviour of the fish for the duration of the
1166 experiment. After the test, fish were returned to their home tanks. The fish tracking was
1167 used to calculate the time spent and the total distance swam in the top area of the tank (top
1168 third of the flask), which were used as measures of anxiety-like behaviour. The more time
1169 spent, and the longer distance swam in the top part of the tank indicate lower anxiety levels.
1170 Moreover, the total distance swam throughout the entire tank was used as a measure of
1171 general motor capacity. This was used as a control to test whether differences in distance
1172 swam in the top part of the tank identified between groups was not due to a potential
1173 locomotive defect but likely associated with an anxiety-like phenotype.
1174

1175 **18. Edu Pulse chase experiment and analysis**

1176 EdU pulse chase was performed as described [72,101]. In brief, fish were fasted for 18 h then
1177 anaesthetised in 4% MS-222 (Covetrus, pharmaceutical grade) injected Intraperitoneally (IP)
1178 with 5ul 10mM EdU ((Click it EdU Alexa Fluour 647 Imaging Kit (Invitrogen, C10340)) or
1179 control solution ((Hanks' Balanced Salt Solution (HBSS) (Gibco, 14,175–053)) using a 30G
1180 3 ml insulin syringe (BD Micro-Fine U-100 insulin, REF 324,826). Fish were injected once
1181 every day for 3 consecutive days at the same time of day (3-day pulse) and culled on day 4
1182 (1 day chase), for paraffin embedding, sectioning and IF (*N* = 4 for each genotype/age).

1183 Immunofluorescent images were processed using ImageJ Fiji (v1.54p) and QuPath (v0.6.0).
1184 Maximum intensity Z-projections were generated, with a minimum of three projections

1185 analysed per animal. Total cell counts were obtained from Channel 1 (DAPI) using QuPath's
1186 automated cell detection. EdU^+ cells (Channel 4) were manually counted, and results were
1187 expressed as the percentage of EdU^+ cells per field of view
1188
1189 **19. Statistical analysis**
1190 All the graphs and respective statistical analysis were performed with GraphPad Prism 7.0.
1191 Normality was assessed by comparing group variances using either the Brown-Forsythe test
1192 or the Shapiro-Wilk normality test. Unpaired t-test or Mann Whitney's unpaired t-test were
1193 used to compare 2 groups, depending on whether the samples presented a Gaussian
1194 distribution or not, respectively. For groups with normal distribution, comparisons over-time
1195 were performed using ANOVA, followed by Turkey test for multiple comparisons. For groups
1196 that failed the normality tests, non-parametric tests were performed, followed by Dunnett's
1197 test for multiple comparisons. A critical value for significance of $p<0.05$ was used in all the
1198 analysis.
1199
1200 **ACKNOWLEDGEMENTS**

1201 We would like to acknowledge and thank Dr Marcus Keatinge for helping with the
1202 chitotriosidase activity assay. We would like to acknowledge and thank the University of
1203 Sheffield Aquarium staff for the great care they provide to our fish and help with protocols,
1204 fish selection and breeding. We would like to acknowledge and thank the Wolfson Light
1205 Microscopy Facility staff for their support throughout the years with all our imaging needs
1206 and challenges. Finally, we would like to acknowledge John Kemp for critical discussion about
1207 transcriptomic data and hypergeometric analysis and statistics.

1208 This work was generously funded by a University of Sheffield PhD studentship to RRM. This
1209 research was funded in whole, or in part, by Wellcome [206224/Z/17/Z/WT_/Wellcome
1210 Trust/United Kingdom]. For the purpose of open access, the author has applied a CC BY
1211 public copyright licence to any Author Accepted Manuscript version arising from this
1212 submission. CMH was also funded by a Vice Chancellor's Fellowship, The University of
1213 Sheffield and a VIVENSA grant AISRPG2305\32, which cover PSE and CP salaries.

1214 RS is funded by the BBSRC SwbioDTP and CH by BBSRC (BB/Y002504/1).

MR is funded by the CNRS and the ANR ADAGIO (ANR-20-CE44-0010). Thanks to the Bettencourt Schueller Foundation long-term partnership, this work was partly supported by the CRI Core Research Fellowship to Michael Rera for SB salary.

CONFLICT OF INTEREST

The authors declare no competing interests.

AUTHOR CONTRIBUTIONS

Author contributions according to CRediT:

RRM: conceptualisation, data curation, formal analysis, funding acquisition, investigation, methodology, project administration, validation, visualisation, writing

SB: data curation, formal analysis, investigation, methodology, software, validation, visualisation, writing

PSE: data curation, formal analysis, investigation, methodology, validation, writing

RS: data curation, formal analysis, investigation, methodology, writing

NH: data curation, formal analysis, investigation, methodology

CP: data curation, formal analysis, investigation, methodology, writing

GEB: formal analysis, methodology, software

OE: investigation

NM: investigation

MHFW: investigation

ZY: investigation

SM: methodology

AJG: methodology

AG: methodology

HM: data curation, formal analysis, funding acquisition, investigation, methodology

1241 **CH:** data curation, formal analysis, funding acquisition, investigation, methodology

1242 **MR:** data curation, formal analysis, funding acquisition, investigation, methodology, project
1243 administration, software, validation, visualisation, writing

1244 **CMH:** conceptualisation, data curation, formal analysis, funding acquisition, investigation,
1245 methodology, project administration, resources, supervision, validation, writing

1246

1247 **DATA AVAILABILITY STATEMENT**

1248 The dataset and source data generated during and/or analysed during the current study is
1249 either shared as supplementary and source data or is available from the corresponding
1250 author upon reasonable request. The RNA sequencing data from this experiment were
1251 deposited in gene expression omnibus (GEO), accession GSE205601.

1252

1253 **ORCID**

1254 *Raquel R. Martins:* https://orcid.org/0000-0003-3952-8649

1255 *Savandara Besse:* https://orcid.org/0000-0003-2448-4022

1256 *Pam S. Ellis:* https://orcid.org/0000-0002-5915-4739

1257 Rabia Sevil: https://orcid.org/0009-0001-4842-8204

1258 *Naomi Hartopp:* https://orcid.org/0000-0003-4069-6324

1259 *Owain Evans:* https://orcid.org/0009-0000-8493-4983

1260 Ada Jimenez-Gonzales: https://orcid.org/0000-0001-7702-6135

1261 Andrew Grierson: https://orcid.org/0000-0001-7039-6731

1262 *Heather Mortiboys:* https://orcid.org/0000-0001-6439-0579

1263 Chrissy Hammon: https://orcid.org/0000-0002-4935-6724

1264 *Michael Rera:* https://orcid.org/0000-0002-6574-6511

1265 *Catarina M. Henriques:* https://orcid.org/0000-0003-1882-756X

1266

1267 **REFERENCES**

1268 1. Collins, B. *et al.* What will the cardiovascular disease slowdown cost? Modelling the
1269 impact of CVD trends on dementia, disability, and economic costs in England and
1270 Wales from 2020-2029. *PLoS One* **17**, e0268766 (2022).

1271 2. Panca, M. *et al.* Healthcare resource utilisation and costs of agitation in people with
1272 dementia living in care homes in England - The Managing Agitation and Raising QUality
1273 of LifE in Dementia (MARQUE) study. *PLoS One* **14**, e0211953 (2019).

1274 3. Wittenberg, R. *et al.* The costs of dementia in England. *Int J Geriatr Psychiatry* **34**,
1275 1095–1103 (2019).

1276 4. Lemoine, M. The Evolution of the Hallmarks of Aging. *Front Genet* **12**, 693071 (2021).

1277 5. Lopez-Otin, C. *et al.* Hallmarks of aging: An expanding universe. *Cell* **186**, 243–278
1278 (2023).

1279 6. de Lange, T. T-loops and the origin of telomeres. *Nat Rev Mol Cell Biol* **5**, 323–9 (2004).

1280 7. Ferreira, M.G. *et al.* Indecent exposure: when telomeres become uncapped. *Mol Cell*
1281 **13**, 7–18 (2004).

1282 8. Bodnar, A.G. Extension of Life-Span by Introduction of Telomerase into Normal Human
1283 Cells. *Science* **279**, 349–352 (1998).

1284 9. d'Adda di Fagagna, F. *et al.* A DNA damage checkpoint response in telomere-initiated
1285 senescence. *Nature* **426**, 194–8 (2003).

1286 10. Coppe, J.P. *et al.* The senescence-associated secretory phenotype: the dark side of
1287 tumor suppression. *Annu Rev Pathol* **5**, 99–118 (2010).

1288 11. Ovadya, Y. *et al.* Senescent cells: SASPected drivers of age-related pathologies.
1289 *Biogerontology* **15**, 627–42 (2014).

1290 12. Tuttle, C.S.L. *et al.* Senescence in tissue samples of humans with age-related diseases:
1291 A systematic review. *Ageing Res Rev* **68**, 101334 (2021).

1292 13. Dimri, G.P. *et al.* A biomarker that identifies senescent human cells in culture and in
1293 aging skin in vivo. *Proc Natl Acad Sci U S A* **92**, 9363–9367 (1995).

1294 14. Birch, J. *et al.* Senescence and the SASP: many therapeutic avenues. *Genes Dev* **34**,
1295 1565–1576 (2020).

1296 15. Fridlyanskaya, I. *et al.* Senescence as a general cellular response to stress: A mini-
1297 review. *Exp Gerontol* **72**, 124–8 (2015).

1298 16. Blackburn, E.H. *et al.* Human telomere biology: A contributory and interactive factor
1299 in aging, disease risks, and protection. *Science* **350**, 1193–8 (2015).

1300 17. Lee, H.W. *et al.* Essential role of mouse telomerase in highly proliferative organs.
1301 *Nature* **392**, 569–74 (1998).

1302 18. Henriques, C.M. *et al.* Telomerase is required for zebrafish lifespan. *PLoS Genet* **9**,
1303 e1003214 (2013).

1304 19. Anchelin, M. *et al.* Premature aging in telomerase-deficient zebrafish. *Dis Model Mech*
1305 **6**, 1101–12 (2013).

1306 20. Carneiro, M.C. *et al.* Short Telomeres in Key Tissues Initiate Local and Systemic Aging
1307 in Zebrafish. *PLoS Genet* **12**, e1005798 (2016).

1308 21. Lex, K. *et al.* Telomere shortening produces an inflammatory environment that
1309 increases tumor incidence in zebrafish. *Proc Natl Acad Sci U S A* **117**, 15066–15074
1310 (2020).

1311 22. Goodman, W.A. *et al.* Length does not matter: a new take on telomerase reverse
1312 transcriptase. *Arterioscler Thromb Vasc Biol* **31**, 235–6 (2011).

1313 23. Romaniuk, A. *et al.* The non-canonical functions of telomerase: to turn off or not to
1314 turn off. *Mol Biol Rep* (2018).

1315 24. Segal-Bendirdjian, E. *et al.* Non-canonical Roles of Telomerase: Unraveling the
1316 Imbroglio. *Front Cell Dev Biol* **7**, 332 (2019).

1317 25. Sung, Y.H. *et al.* Extracting extra-telomeric phenotypes from telomerase mouse
1318 models. *Yonsei Med J* **55**, 1–8 (2014).

1319 26. Deacon, K. *et al.* PINX1 and TERT Are Required for TNF-alpha-Induced Airway Smooth
1320 Muscle Chemokine Gene Expression. *J Immunol* **200**, 1283–1294 (2018).

1321 27. Ghosh, A. *et al.* Telomerase directly regulates NF-kappaB-dependent transcription.
1322 *Nat Cell Biol* **14**, 1270–81 (2012).

1323 28. Mattiussi, M. *et al.* Human telomerase represses ROS-dependent cellular responses
1324 to Tumor Necrosis Factor-α without affecting NF-κB activation. *Cellular signalling* **24**,
1325 708–17 (2012).

1326 29. Choi, J. *et al.* TERT promotes epithelial proliferation through transcriptional control of
1327 a Myc- and Wnt-related developmental program. *PLoS Genet* **4**, e10 (2008).

1328 30. Sarin, K.Y. *et al.* Conditional telomerase induction causes proliferation of hair follicle
1329 stem cells. *Nature* **436**, 1048–52 (2005).

1330 31. Cao, Y. *et al.* TERT regulates cell survival independent of telomerase enzymatic
1331 activity. *Oncogene* **21**, 3130–8 (2002).

1332 32. Rahman, R. *et al.* hTERT antagonizes p53-induced apoptosis independently of
1333 telomerase activity. *Oncogene* **24**, 1320–7 (2005).

1334 33. Ahmed, S. *et al.* Telomerase does not counteract telomere shortening but protects
1335 mitochondrial function under oxidative stress. *J Cell Sci* **121**, 1046–53 (2008).

1336 34. Haendeler, J. *et al.* Mitochondrial telomerase reverse transcriptase binds to and
1337 protects mitochondrial DNA and function from damage. *Arterioscler Thromb Vasc Biol*
1338 **29**, 929–35 (2009).

1339 35. Eitan, E. *et al.* Novel telomerase-increasing compound in mouse brain delays the onset
1340 of amyotrophic lateral sclerosis. *EMBO Mol Med* **4**, 313–29 (2012).

1341 36. Spilsbury, A. *et al.* The role of telomerase protein TERT in Alzheimer's disease and in
1342 tau-related pathology in vitro. *J Neurosci* **35**, 1659–74 (2015).

1343 37. Lee, J. *et al.* Telomerase deficiency affects normal brain functions in mice. *Neurochem*
1344 *Res* **35**, 211–8 (2010).

1345 38. De Felice, B. *et al.* Telomerase expression in amyotrophic lateral sclerosis (ALS)
1346 patients. *J Hum Genet* **59**, 555–61 (2014).

1347 39. Jaskelioff, M. *et al.* Telomerase reactivation reverses tissue degeneration in aged
1348 telomerase-deficient mice. *Nature* **469**, 102–106 (2011).

1349 40. Jurk, D. *et al.* Postmitotic neurons develop a p21-dependent senescence-like
1350 phenotype driven by a DNA damage response. *Aging Cell* **11**, 996–1004 (2012).

1351 41. Raj, D.D.A. *et al.* Enhanced microglial pro-inflammatory response to
1352 lipopolysaccharide correlates with brain infiltration and blood-brain barrier
1353 dysregulation in a mouse model of telomere shortening. *Aging Cell*, 1003–1013
1354 (2015).

1355 42. Hernandez-Segura, A. *et al.* Hallmarks of Cellular Senescence. *Trends Cell Biol* **28**, 436–
1356 453 (2018).

1357 43. Tripathi, U. *et al.* Impact of Senescent Cell Subtypes on Tissue Dysfunction and Repair:
1358 Importance and Research Questions. *Mech Ageing Dev* **198**, 111548 (2021).

1359 44. Yu, X. *et al.* Telomerase reverse transcriptase and neurodegenerative diseases. *Front*
1360 *Immunol* **14**, 1165632 (2023).

1361 45. Papageorgakopoulou, M.A. *et al.* The Role of Glia Telomere Dysfunction in the
1362 Pathogenesis of Central Nervous System Diseases. *Mol Neurobiol* **61**, 5868–5881
1363 (2024).

1364 46. Vellingiri, B. *et al.* Role of Telomeres and Telomerase in Parkinson's Disease-A New
1365 Theranostics? *Adv Biol (Weinh)* **7**, e2300097 (2023).

1366 47. Topiwala, A. *et al.* Telomere length and brain imaging phenotypes in UK Biobank. *PLoS*
1367 *One* **18**, e0282363 (2023).

1368 48. Bhat, R. *et al.* Astrocyte senescence as a component of Alzheimer's disease. *PLoS One*
1369 **7**, e45069 (2012).

1370 49. Chinta, S.J. *et al.* Cellular Senescence Is Induced by the Environmental Neurotoxin
1371 Paraquat and Contributes to Neuropathology Linked to Parkinson's Disease. *Cell Rep*
1372 **22**, 930–940 (2018).

1373 50. Gaikwad, S. *et al.* Senescence, brain inflammation, and oligomeric tau drive cognitive
1374 decline in Alzheimer's disease: Evidence from clinical and preclinical studies.
1375 *Alzheimers Dement* **20**, 709–727 (2024).

1376 51. Bussian, T.J. *et al.* Clearance of senescent glial cells prevents tau-dependent pathology
1377 and cognitive decline. *Nature* **562**, 578–582 (2018).

1378 52. Forsyth, N.R. *et al.* Telomerase and differentiation in multicellular organisms: turn it
1379 off, turn it on, and turn it off again. *Differentiation* **69**, 188–97 (2002).

1380 53. Gomes, N.M. *et al.* Comparative biology of mammalian telomeres: hypotheses on
1381 ancestral states and the roles of telomeres in longevity determination. *Aging Cell* **10**,
1382 761–8 (2011).

1383 54. Henriques, C.M. *et al.* Consequences of telomere shortening during lifespan. *Curr Opin*
1384 *Cell Biol* **24**, 804–8 (2012).

1385 55. Sprungala, S. Telomere length, telomerase and maintenance of stem cells in
1386 the adult zebrafish brain. (TECHNISCHE UNIVERSITÄT MÜNCHEN, 2009).

1387 56. Zambusi, A. *et al.* Granulins Regulate Aging Kinetics in the Adult Zebrafish
1388 Telencephalon. *Cells* **9**(2020).

1389 57. Carneiro, M.C. *et al.* Short Telomeres in Key Tissues Initiate Local and Systemic Aging
1390 in Zebrafish. *PLoS genetics* **12**, e1005798 (2016).

1391 58. Hayflick, L. Biological aging is no longer an unsolved problem. *Ann N Y Acad Sci* **1100**,
1392 1–13 (2007).

1393 59. Rando, T.A. *et al.* Asynchronous, contagious and digital aging. *Nat Aging* **1**, 29–35
1394 (2021).

1395 60. Schaum, N. *et al.* Ageing hallmarks exhibit organ-specific temporal signatures. *Nature*
1396 **583**, 596–602 (2020).

1397 61. Tabula Muris, C. A single-cell transcriptomic atlas characterizes ageing tissues in the
1398 mouse. *Nature* **583**, 590–595 (2020).

1399 62. Zhang, M.J. *et al.* Mouse aging cell atlas analysis reveals global and cell type-specific
1400 aging signatures. *Elife* **10**(2021).

1401 63. Lawson, N.D. *et al.* An improved zebrafish transcriptome annotation for sensitive and
1402 comprehensive detection of cell type-specific genes. *Elife* **9**(2020).

1403 64. Ernst, J. *et al.* STEM: a tool for the analysis of short time series gene expression data.
1404 *BMC Bioinformatics* **7**, 191 (2006).

1405 65. Anneser, L. *et al.* Molecular organization of neuronal cell types and neuromodulatory
1406 systems in the zebrafish telencephalon. *Curr Biol* **34**, 298–312 e4 (2024).

1407 66. Zane, F. *et al.* Smurfness-based two-phase model of ageing helps deconvolve the
1408 ageing transcriptional signature. *Aging Cell* **22**, e13946 (2023).

1409 67. Frenk, S. *et al.* Gene expression hallmarks of cellular ageing. *Biogerontology* **19**, 547–
1410 566 (2018).

1411 68. Huang, W. *et al.* Cellular senescence: the good, the bad and the unknown. *Nat Rev*
1412 *Nephrol* **18**, 611–627 (2022).

1413 69. Vazquez-Villasenor, I. *et al.* Expression of p16 and p21 in the frontal association cortex
1414 of ALS/MND brains suggests neuronal cell cycle dysregulation and astrocyte
1415 senescence in early stages of the disease. *Neuropathol Appl Neurobiol* **46**, 171–185
1416 (2020).

1417 70. Martin-Ruiz, C. *et al.* Senescence and Inflammatory Markers for Predicting Clinical
1418 Progression in Parkinson's Disease: The ICICLE-PD Study. *J Parkinsons Dis* **10**, 193–206
1419 (2020).

1420 71. Idda, M.L. *et al.* Survey of senescent cell markers with age in human tissues. *Aging*
1421 *(Albany NY)* **12**, 4052–4066 (2020).

1422 72. Ellis, P.S. *et al.* A subset of gut leukocytes has telomerase-dependent "hyper-long"
1423 telomeres and require telomerase for function in zebrafish. *Immun Ageing* **19**, 31
1424 (2022).

1425 73. Saul, D. *et al.* A new gene set identifies senescent cells and predicts senescence-
1426 associated pathways across tissues. *Nat Commun* **13**, 4827 (2022).

1427 74. Basisty, N. *et al.* A proteomic atlas of senescence-associated secretomes for aging
1428 biomarker development. *PLoS Biol* **18**, e3000599 (2020).

1429 75. Ellett, F. *et al.* mpeg1 promoter transgenes direct macrophage-lineage expression in
1430 zebrafish. *Blood* **117**, e49–56 (2011).

1431 76. Oosterhof, N. *et al.* Identification of a conserved and acute neurodegeneration-
1432 specific microglial transcriptome in the zebrafish. *Glia* **65**, 138–149 (2017).

1433 77. Cvejic, A. *et al.* Analysis of WASp function during the wound inflammatory response--
1434 live-imaging studies in zebrafish larvae. *J Cell Sci* **121**, 3196–206 (2008).

1435 78. Mathias, J.R. *et al.* Characterization of Zebrafish Larval Inflammatory Macrophages
1436 Jonathan. *Developmental and Comparative Immunology* **33**, 1212–1217 (2010).

1437 79. Redd, M.J. *et al.* Imaging macrophage chemotaxis in vivo: studies of microtubule
1438 function in zebrafish wound inflammation. *Cell Motil Cytoskeleton* **63**, 415–22 (2006).

1439 80. Van Houcke, J. *et al.* Successful optic nerve regeneration in the senescent zebrafish
1440 despite age-related decline of cell intrinsic and extrinsic response processes.
1441 *Neurobiol Aging* **60**, 1–10 (2017).

1442 81. Martins, R.R. *et al.* Resident Immunity in Tissue Repair and Maintenance: The
1443 Zebrafish Model Coming of Age. *Front Cell Dev Biol* **7**, 12 (2019).

1444 82. Deleidi, M. *et al.* Immune aging, dysmetabolism, and inflammation in neurological
1445 diseases. *Front Neurosci* **9**, 172 (2015).

1446 83. Franceschi, C. *et al.* Chronic inflammation (inflammaging) and its potential
1447 contribution to age-associated diseases. *J Gerontol A Biol Sci Med Sci* **69 Suppl 1**, S4–
1448 9 (2014).

1449 84. Figueira, I. *et al.* Interventions for age-related diseases: Shifting the paradigm. *Mech*
1450 *Ageing Dev* **160**, 69–92 (2016).

1451 85. Demaria, M. *et al.* An Essential Role for Senescent Cells in Optimal Wound Healing
1452 through Secretion of PDGF-AA. *Developmental Cell* **31**, 722–733 (2014).

1453 86. Krizhanovsky, V. *et al.* Implications of cellular senescence in tissue damage response,
1454 tumor suppression, and stem cell biology. *Cold Spring Harb Symp Quant Biol* **73**, 513–
1455 22 (2008).

1456 87. Acosta, J.C. *et al.* A complex secretory program orchestrated by the inflammasome
1457 controls paracrine senescence. *Nature cell biology* **15**, 978–90 (2013).

1458 88. Muldoon, L.L. *et al.* Immunologic privilege in the central nervous system and the
1459 blood-brain barrier. *J Cereb Blood Flow Metab* **33**, 13–21 (2013).

1460 89. Fleming, A. *et al.* Functional characterisation of the maturation of the blood-brain
1461 barrier in larval zebrafish. *PLoS One* **8**, e77548 (2013).

1462 90. Jeong, J.Y. *et al.* Functional and developmental analysis of the blood-brain barrier in
1463 zebrafish. *Brain Res Bull* **75**, 619–28 (2008).

1464 91. Bassi, G.S. *et al.* Lipopolysaccharide-induced sickness behaviour evaluated in different
1465 models of anxiety and innate fear in rats. *Basic Clin Pharmacol Toxicol* **110**, 359–69
1466 (2012).

1467 92. Tarr, A.J. *et al.* Neural and behavioral responses to low-grade inflammation. *Behav*
1468 *Brain Res* **235**, 334–41 (2012).

1469 93. Wong, K. *et al.* Analyzing habituation responses to novelty in zebrafish (Danio rerio).
1470 *Behav Brain Res* **208**, 450–7 (2010).

1471 94. Kalueff, A. *The rights and wrongs of zebrafish: Behavioral phenotyping of zebrafish*,
1472 (2017).

1473 95. Righi, D. *et al.* Investigating interleukin-8 in Alzheimer's disease: A comprehensive
1474 review. *J Alzheimers Dis* **103**, 38–55 (2025).

1475 96. Samant, R.R. *et al.* The emerging role of disease-associated microglia in Parkinson's
1476 disease. *Front Cell Neurosci* **18**, 1476461 (2024).

1477 97. Lujambio, A. To clear, or not to clear (senescent cells)? That is the question. *Bioessays*
1478 **38 Suppl 1**, S56–64 (2016).

1479 98. Chen, Y. *et al.* Macrophage-derived CTSS drives the age-dependent disruption of the
1480 blood-CSF barrier. *Neuron* **113**, 1082–1097 e8 (2025).

1481 99. Wong, R.Y. *et al.* Limited sex-biased neural gene expression patterns across strains in
1482 Zebrafish (Danio rerio). *BMC Genomics* **15**, 905 (2014).

1483 100. Keatinge, M. *et al.* Glucocerebrosidase 1 deficient Danio rerio mirror key pathological
1484 aspects of human Gaucher disease and provide evidence of early microglial activation
1485 preceding alpha-synuclein-independent neuronal cell death. *Hum Mol Genet* (2015).

1486 101. Martins, R.R., Zamzam, M.,Tracey-White, D., Moosajee, M., Thummel, R., Henriques,
1487 C.M., & MacDonald, R. B. . Müller Glia maintain theirregenerative potential despite
1488 degeneration in the aged zebrafish retina. *Aging Cell* (2022).
1489